Landscape fire smoke airway exposure impairs respiratory and cardiac function and worsens experimental asthma

Henry M. Gomez, PhD, Tatt J. Haw, PhD, Dusan Ilic, PhD, Peter Robinson, PhD, Chantal Donovan, PhD, Amanda J. Croft, et al

GRAPHICAL ABSTRACT

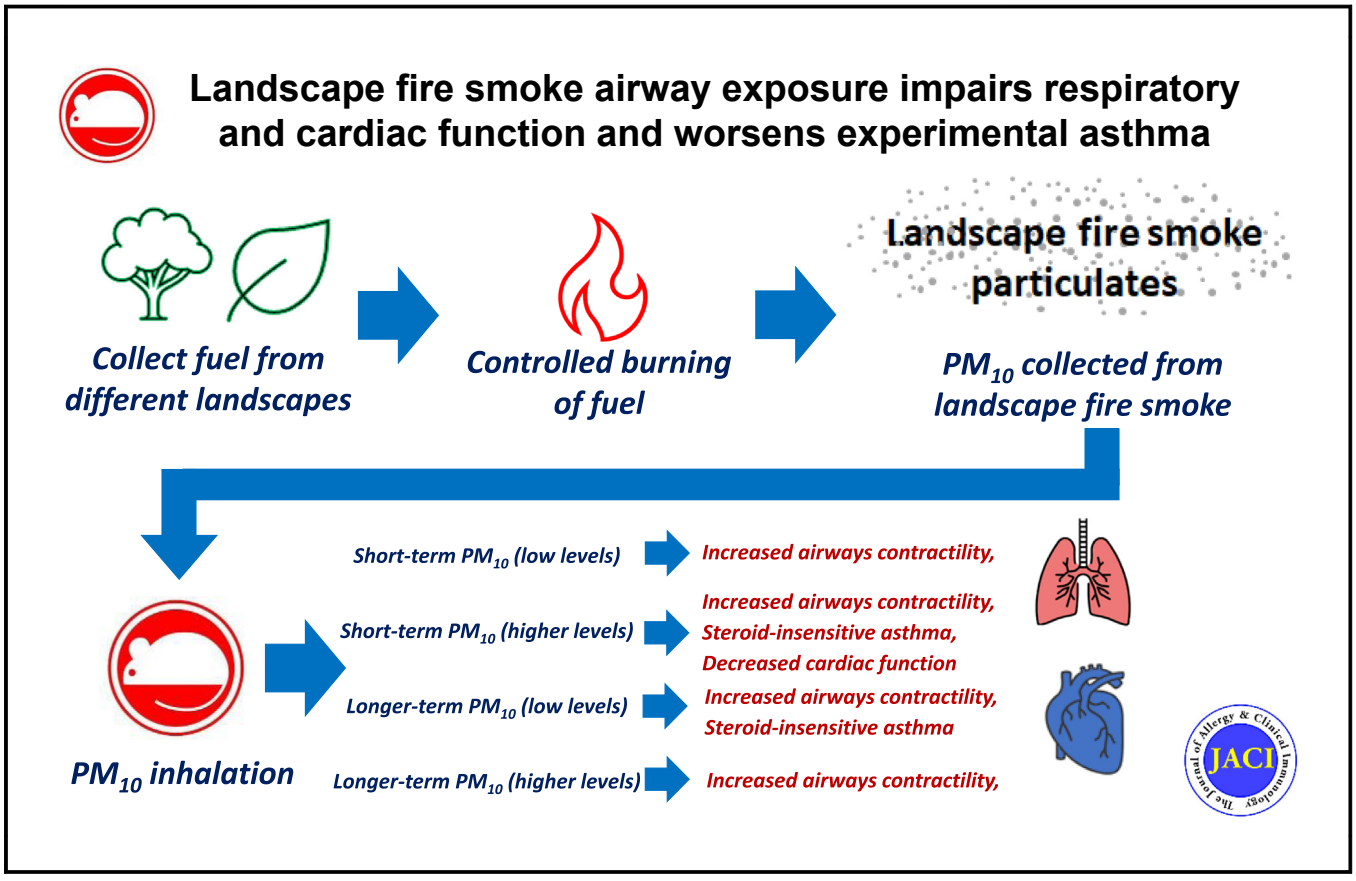

Capsule summary: Landscape fire smoke exposure worsens respiratory disease and cardiovascular outcomes.

J Allergy Clin Immunol 2024;154:209-21.

https://doi.org/10.1016/j.jaci.2024.02.022

Landscape fire smoke airway exposure impairs respiratory and cardiac function and worsens experimental asthma

Henry M. Gomez, PhD,[a] Tatt J. Haw, PhD,[b,c] Dusan Ilic, PhD,[d] Peter Robinson, PhD,[d] Chantal Donovan, PhD,[a,e] Amanda J. Croft,[b,c] Kanth S. Vanka, PhD,[a,d] Ellen Small, BBiomed,[a] Olivia R. Carroll, BBiomed,[a] Richard Y. Kim, PhD,[a,e] Jemma R. Mayall, PhD,[a] Tesfalidet Beyene, PhD,[f] Thava Palanisami, PhD,[g] Doan T. M. Ngo, PhD,[b,c] Graeme R. Zosky, PhD,[h,i] Elizabeth G. Holliday, PhD,[j] Megan E. Jensen, PhD,[f] Vanessa M. McDonald, PhD,[f] Vanessa E. Murphy, PhD,[f] Peter G. Gibson, MBBS, DMed, FRACP,[f] and Jay C. Horvat, PhD[a]

Newcastle, Callaghan, Sydney, and Hobart, Australia

Background: Millions of people are exposed to landscape fire smoke (LFS) globally, and inhalation of LFS particulate matter (PM) is associated with poor respiratory and cardiovascular outcomes. However, how LFS affects respiratory and cardiovascular function is less well understood.

Objective: We aimed to characterize the pathophysiologic effects of representative LFS airway exposure on respiratory and cardiac function and on asthma outcomes.

Methods: LFS was generated using a customized combustion chamber. In 8-week-old female BALB/c mice, low (25 μg/m^3, 24-hour equivalent) or moderate (100 μg/m^3, 24-hour equivalent) concentrations of LFS PM (10 μm and below [PM_{10}]) were administered daily for 3 (short-term) and 14 (long-term) days in the presence and absence of experimental asthma. Lung inflammation, gene expression, structural changes, and lung function were assessed. In 8-week-old male C57BL/6 mice, low concentrations of LFS PM_{10} were administered for 3 days. Cardiac function and gene expression were assessed.

Results: Short- and long-term LFS PM_{10} airway exposure increased airway hyperresponsiveness and induced steroid insensitivity in experimental asthma, independent of significant changes in airway inflammation. Long-term LFS PM_{10} airway exposure also decreased gas diffusion. Short-term LFS PM_{10} airway exposure decreased cardiac function and expression of gene changes relating to oxidative stress and cardiovascular pathologies.

Conclusions: We characterized significant detrimental effects of physiologically relevant concentrations and durations of LFS PM_{10} airway exposure on lung and heart function. Our study provides a platform for assessment of mechanisms that underpin LFS PM_{10} airway exposure on respiratory and cardiovascular disease outcomes. (J Allergy Clin Immunol 2024;154:209-21.)

Key words: *Landscape fire smoke, particulate matter exposure, air pollution, lung disease, cardiovascular disease, asthma*

Landscape fires are becoming more frequent and intense globally, exposing millions of people to hazardous levels of landscape fire smoke (LFS) particulate matter (PM).[1] The 2019-2020 Australian landscape fire season resulted in more than 12.6 million hectares of land being burned and released millions of tons of smoke and gases into the atmosphere.[2] Pollution from landscape fires is associated with increased respiratory- and cardiac-associated emergency department presentations and admissions,[3] and patients with asthma are disproportionately affected by LFS exposure compared with individuals without asthma.[2,4,5]

The pathophysiologic mechanisms that underpin the respiratory and cardiovascular manifestations of LFS airway exposure are not well understood, and the development of effective therapies is predicated on improving our understanding of LFS airway exposure–induced responses. To our knowledge, no studies to date have used naturally occurring sources of geography-specific vegetation to account for the heterogeneity of real-world LFS. Real-world exposure to LFS may vary in terms of duration and concentration, with longer-term lower exposures and shorter-term moderate to high exposures experienced during the 2019-2020 Australian landscape fire season and worldwide. Moreover, LFS PM is heterogeneous in terms of particulate size distribution and chemical and elemental composition[6,7] and can be influenced by fuel source, loads, and burn conditions (oxygen availability, moisture content, and prevailing winds). LFS PM with a diameter of 10 μm and below (PM_{10}) induces responses in the upper airway and includes the subfractions of $PM_{2.5}$ and $PM_{0.1}$ that travel deeper into the lungs and are absorbed systemically.

From [a]School of Biomedical Sciences and Pharmacy, University of Newcastle and Immune Health Program, Hunter Medical Research Institute, Newcastle; [b]Heart and Stroke Research Program, Hunter Medical Research Institute, New Lambton Heights, Newcastle; [c]College of Health, Medicine, and Wellbeing, Centre of Excellence Newcastle Cardio-Oncology Research Group, University of Newcastle, Callaghan, Newcastle; [d]Newcastle Institute for Energy and Resources, University of Newcastle, Callaghan; [e]School of Life Sciences, University of Technology Sydney, Faculty of Science, Sydney; [f]School of Medicine and Public Health, University of Newcastle and Asthma and Breathing Program, Hunter Medical Research Institute, Newcastle; [g]Global Innovative Centre for Advanced Nanomaterials, University of Newcastle, Callaghan; [h]Menzies Institute for Medical Research, College of Health and Medicine, University of Tasmania, Hobart; [i]College of Health and Medicine, Tasmanian School of Medicine, University of Tasmania, Hobart; and [j]School of Medicine and Public Health, University of Newcastle, Callaghan.

Received for publication May 9, 2023; revised February 13, 2024; accepted for publication February 22, 2024.

Available online March 19, 2024.

Corresponding author: Jay C. Horvat, PhD, Level 2 East, Hunter Medical Research Institute, Lot 1 Kookaburra Court New Lambton Heights, New South Wales 2305, Australia. E-mail: jay.horvat@newcastle.edu.au.

0091-6749

https://doi.org/10.1016/j.jaci.2024.02.022

Abbreviations used
AHR: Airway hyperresponsiveness
BAL: Bronchoalveolar lavage
DEX: Dexamethasone
DF_{CO}: Diffusing factor of the lung for carbon monoxide
GC-MS: Gas chromatography mass spectrometry
ICP-MS: Inductively coupled mass spectrometry
LFS: Landscape fire smoke
LV: Left ventricular
OVA: Ovalbumin
PAH: Polycyclic aromatic hydrocarbon
PCLS: Precision cut lung slices
PM: Particulate matter
sHBSS: Sterile Hanks' Balanced Salt Solution

In this study, we developed a novel and safe method to generate and capture vegetation-specific LFS PM_{10} and deliver physiologically representative concentrations to mice. We aimed to characterize the effects of LFS PM_{10} airway exposure on airway hyperresponsiveness (AHR) in healthy mice and in steroid insensitivity in experimental asthma, proinflammatory cytokine responses in lung and heart tissues, and cardiac function.

METHODS

Generation and characterization of LFS PM_{10} for *in vivo* delivery at representative levels

Vegetation from 2 native Australian trees, *Corymbia maculata* (spotted gum) and *Callistemon citrinus* (red bottlebrush), was collected from the University of Newcastle, Australia, dried (45°C, 72 hours), and placed into a combustion chamber (20 minutes under positive pressure [30 L/minute]) (fuel source 1). LFS particulates and gases were fed into a bottle of dry ice supercooled pure water. Effluent gases were ducted into an extraction hood (capture velocity > 0.5 m/second as per Australian/New Zealand Standard AS/NZS 2243.8-2006). Particulates in solution were drip fed through a Whatman Grade 1 filter paper (Cytiva, Buckinghamshire, United Kingdom) to isolate the PM_{10} fraction. Aliquots of the resultant particulate solution (LFS PM_{10}) were evaporated in glass tubes using the Genevac miVac Duo Concentrator (10 mbar, 16 hours; Genevac, Ipswich, United Kingdom) and dried (100°C, 12 hours), and total particulate mass per unit volume was calculated. A second sample of bushfire smoke particulates (fuel source 2) was generated from equal proportions of leaves, twigs, and bark from 2 species of tree, *Eucalyptus punctata* (grey gum) and *Eucalyptus fibrosa* (broad-leaved ironbark); a shrub, *Persoonia linearis* (narrow-leaved geebung); and a grass, *Entolasia stricta* (wiry panic). These 4 species were collected from localities within greater Newcastle and represent flora commonly found within the Wollomi National Park, which was significantly burned during the 2019-2020 fire season and contributed to the smoke air pollution experienced by Newcastle, Australia during this time.

Metal(loid) concentration was assessed using inductively coupled plasma mass spectroscopy (ICP-MS), and polycyclic aromatic hydrocarbons (PAHs) were assessed using gas chromatography mass spectrometry (GC-MS) (detailed in this article's Methods section in the Online Repository at www.jacionline.org).

LFS PM_{10} airway exposure in the absence and presence of experimental asthma

All mice (Central Animal House, University of Newcastle, Newcastle, Australia) were housed in specific pathogen-free, Physical Containment Level 2 conditions in individually ventilated cages (bioresources facility, Hunter Medical Research Institute, Newcastle, Australia) and provided with food and water *ad libitum*. All experiments were performed on mice 8 to 12 weeks of age, with age-matched controls included within each experimental run. All studies were performed with approval from the Animal Care and Ethics Committee of the University of Newcastle.

To assess human-relevant LFS PM_{10} airway exposure, female BALB/c mice (n = 6-11) received the equivalent of low (25 μg/m^3/0.1152 μg) or moderate (100 μg/m^3/0.4608 μg) LFS PM_{10} over a 24-hour period in 50 μL PBS, each day for 3 days (short-term) or 14 days (long-term) by intranasal administration (Fig E1, *A* and *B*, in the Online Repository at www.jacionline.org). Determination of representative concentrations and calculations of human-relevant, mouse-normalized exposures of LFS PM_{10} are outlined in the Methods section in the Online Repository.

To assess the effects of LFS PM_{10} airway exposure on asthma severity, female BALB/c mice were treated with ovalbumin (OVA) in the absence or presence of corticosteroid (dexamethasone [DEX]) as previously described.[8-11] Briefly, mice were sensitized to OVA (50 μg; Sigma-Aldrich, Castle Hill, New South Wales, Australia), with the adjuvant alum (1 mg Rehydrogel [Reheis, Berkeley Heights, NJ] in 200 μL 0.9% saline, intraperitoneal injection) on day 0. Mice were then intranasally challenged with OVA on days 12 and 13 and days 33 and 34 (10 μg and 50 μL saline) (Fig E1, *C*). Controls were sham sensitized with alum alone and intranasally treated with OVA on days 12 and 13 and days 33 and 34. To model the effects of LFS PM_{10} airway exposure on asthma, some groups of mice were intranasally administered 25 μg/m^3 LFS PM_{10} on days 20 to 34 or 100 μg/m^3 LFS PM_{10} on days 32 to 34 (Fig E1, *C*). To model the effects of inhaled corticosteroids, some groups of mice were intranasally administered DEX (2 mg/kg in PBS, #D1756; Sigma-Aldrich) on days 32 to 34. Controls for LFS and DEX interventions were intranasally administered PBS (50 μL). Lung function and airway inflammation were assessed on day 35 (Fig E1, *C*).

Assessment of lung function

A single breath hold maneuver to assess the effect of LFS PM_{10} airway exposure on gas exchange (diffusing factor of the lung for carbon monoxide [DF_{CO}]) was performed on short- and long-term models (Fig E1, *A* and *B*) as previously described.[12,13] AHR to methacholine was also measured in all models using the flexiVent FX1 system (SCIREQ, Montreal, Quebec, Canada) as previously described.[8,14-16]

Airway inflammation, alveolar diameter, and collagen deposition

Airway inflammation was measured in bronchoalveolar lavage (BAL) fluid as previously described.[14-17] Alveolar diameter and collagen deposition around the small airway were measured in histologic sections of paraffin-embedded tissues as previously described.[14-17]

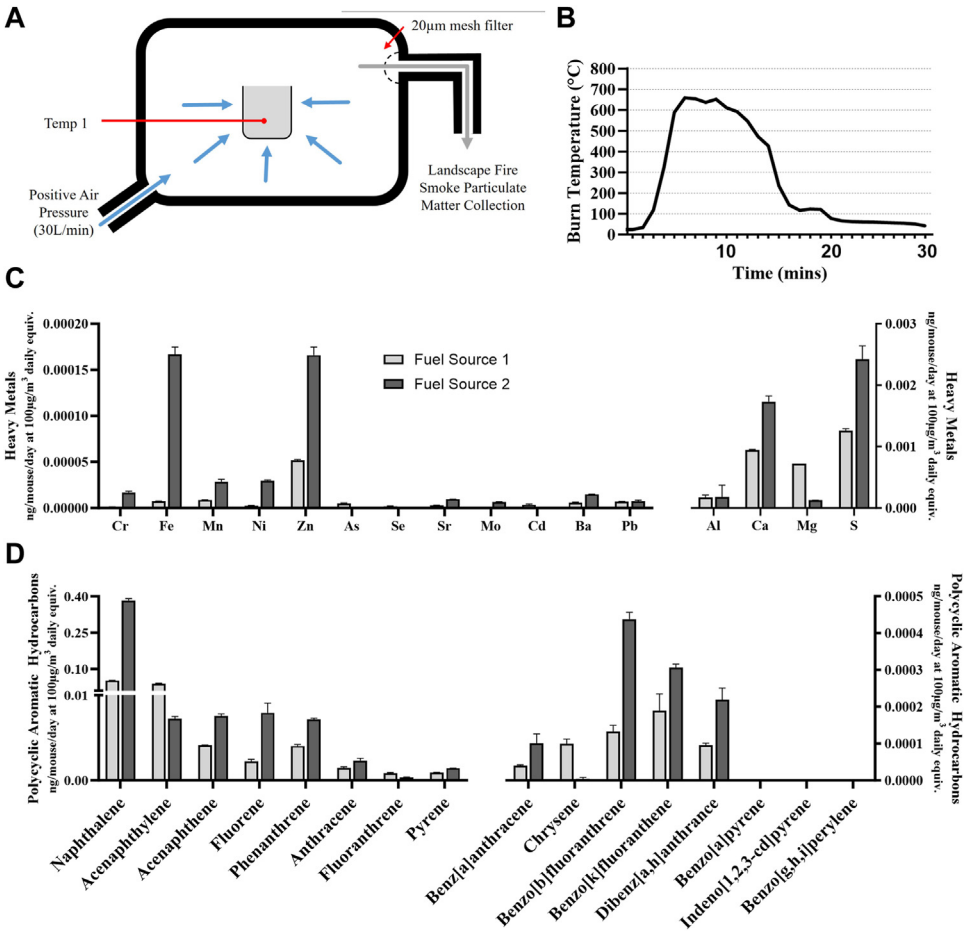

FIG 1. Characterization of vegetation-specific LFS PM_{10}. **(A)** Customized combustion chamber used to generate LFS PM_{10}. **(B)** Temperature burn profile as measured by a thermocouple situated inside the combustion chamber. **(C)** Heavy metal composition of fuel source 1 and fuel source 2 as measured by ICP-MS represented as total mass in 50 μL administered intranasally at 100 $\mu g/m^3$ concentration. **(D)** Polycyclic aromatic hydrocarbon abundance of fuel source 1 and fuel source 2 as measured by GC-MS represented as total mass in 50 μL administered intranasally at 100 $\mu g/m^3$ concentration.

Cardiac function assessments

Echocardiograph analysis was also performed on a separate group of male C57BL/6 mice (n = 7-8) before and after 3 days of short-term/moderate LFS PM_{10} airway exposure as previously described in BALB/c mice (Fig E1, *D*).[18] C57BL/6 mice were used for ethical reasons, as this technique has been established only in this strain in our laboratory. Left ventricular (LV) dimensions, systolic function, and diastolic function (E/A ratio, LV fractional shortening, and LV ejection fraction) were assessed with transmitral and tissue Doppler echocardiography with the use of a VisualSonics Vevo 1100 (FUJIFILM VisualSonics, Inc., Toronto, Ontario, Canada) high-resolution imaging system as previously described.[18]

Airway contractility and cilia beat frequency

Airway contractility and cilia beat frequency were assessed in precision cut lung slices generated from a subset of mice after short-term/moderate LFS PM_{10} airway exposure with and without DEX treatment (Fig E1, *C*), as previously described[13,19-21] detailed in the Methods section in the Online Repository.

RNA extraction, reverse transcription, and gene expression analyses

Whole lung and/or heart tissues from subsets of mice (n = 6-8) were collected in Invitrogen RNAlater Stabilization Solution (AM7021; Thermo Fisher Scientific, Waltham, Mass), stored overnight at 4°C, and stored long-term at −20°C. For RNA extraction, samples were transferred to 1 mL TRI Reagent (T9424; Sigma Aldrich) and homogenized using 5-mm stainless steel beads (#69989; QIAGEN, Hilden, Germany) and a TissueLyser II (QIAGEN). Total RNA was reverse transcribed as previously described.[11,16,22] Gene expression was measured using SYBR Green Assay (Bio-Rad Laboratories, Hercules, Calif), predesigned primers (Table E1 in the Online Repository at www.jacionline.org) using the BioRad CFX384 system as previously described.[11,16,22] Relative mRNA expression of genes of interest were normalized to the reference gene *Hprt* (for lung) or *Ppia* (for heart) using the following calculation:

Relative expression = 2 ^ − (housekeeper Ct − gene of interest Ct)

where Ct is the cycle threshold.

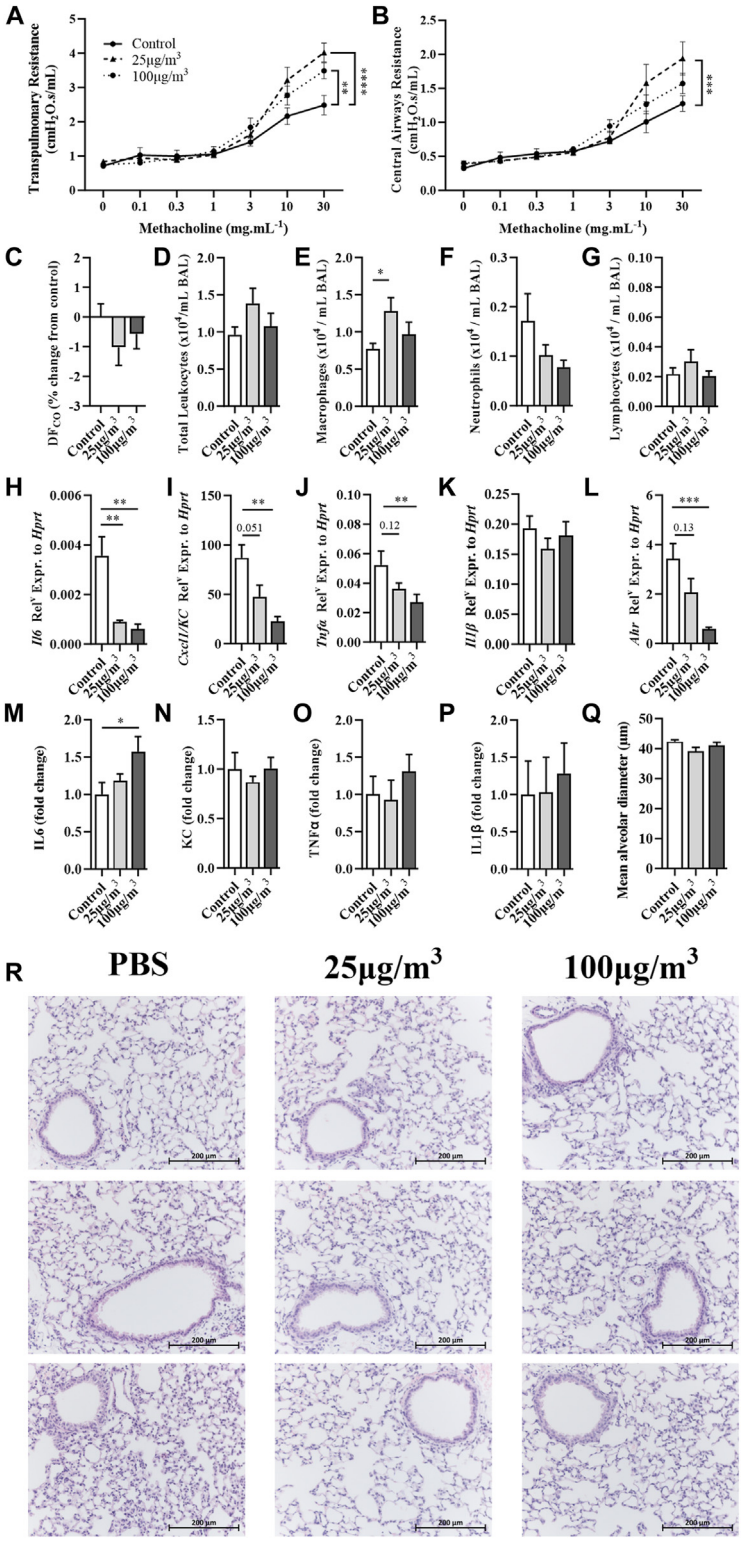

FIG 2. Short-term LFS PM_{10} airway exposure alters lung function, independent of airway inflammation, and suppresses inflammatory gene expression. Following short-term (3 days) airway exposure to PBS (control), 25 $\mu g/m^3$ LFS PM_{10} (low; daily equivalent), or 100 $\mu g/m^3$ LFS PM_{10} (moderate; daily equivalent), AHR was measured in response to increasing concentrations of nebulized methacholine in terms of **(A)** transpulmonary resistance, **(B)** central airway resistance, and **(C)** DF_{CO}. Inflammation of the airway was measured in BAL **(D)** total leukocytes, **(E)** macrophages, **(F)** neutrophils, and **(G)** lymphocytes. mRNA expression of **(H)** *Il6,* **(I)** *Cxcl1/KC,* **(J)** *Tnfα*, **(K)** *Il1β*, and **(L)** *Ahr* was measured in whole lung homogenate, and **(M)** IL-6, **(N)** CXCL1/KC, **(O)** TNF-α, and **(P)** IL-1β protein expression was measured in BAL fluid. **(Q)** Mean alveolar diameter was assessed with **(R)** representative photomicrographs (scale bar, 200 μm) showing inflammatory cells near airway and surrounding parenchyma. Two-way ANOVA was performed for *(A* and *B)*. Unpaired *t* tests were performed on LFS PM_{10} groups compared with controls for (*C-Q*). n = 5-11/group. Data presented as mean ± SEM. **P* < .05, ***P* < .01, ****P* < .001, *****P* < .0001.

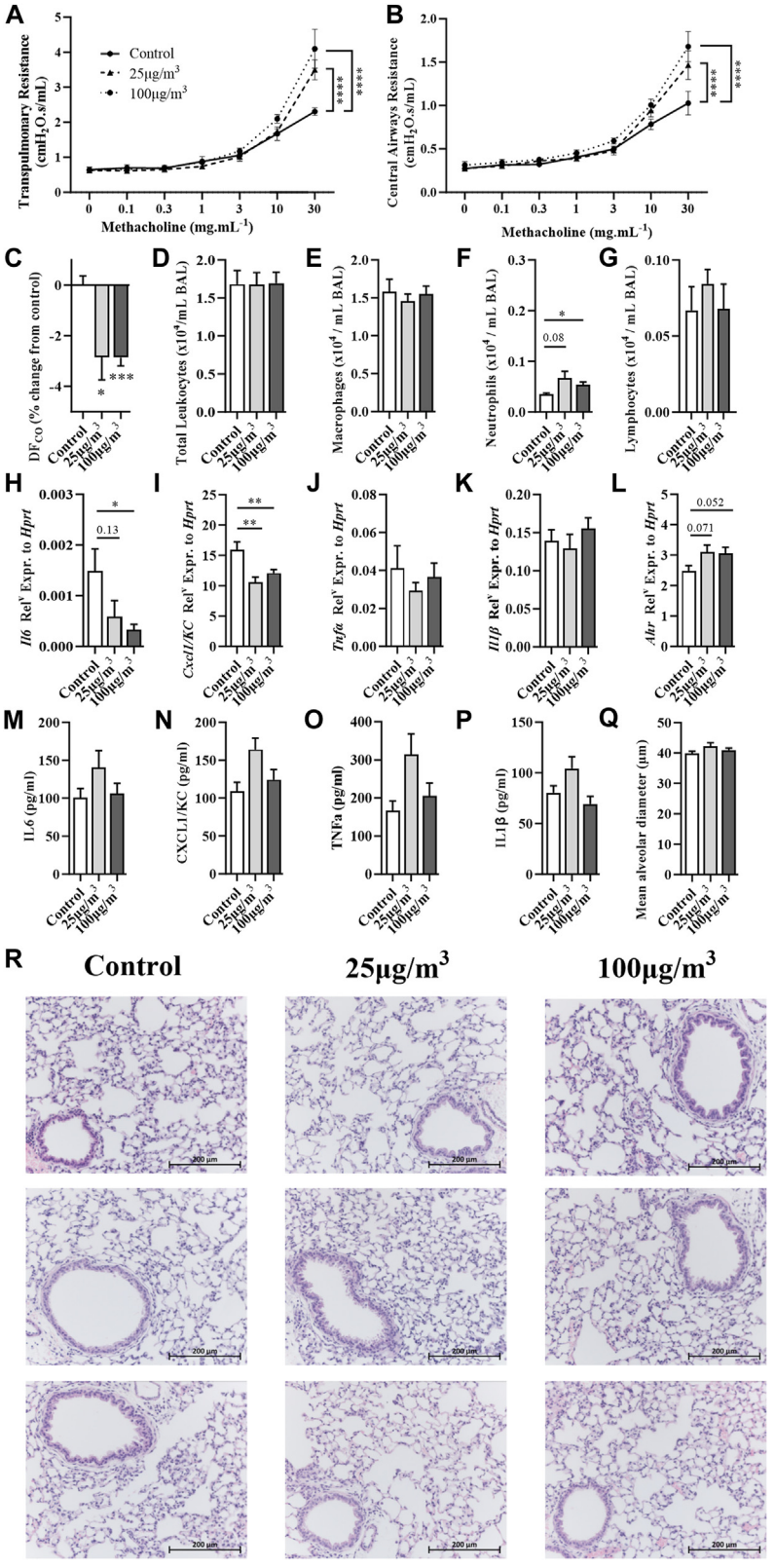

FIG 3. Long-term LFS PM_{10} airway exposure increases AHR, impairs gas exchange, and suppresses mRNA expression of proinflammatory mediators in the lung. Following long-term (14 days) airway exposure to PBS (control), 25 $\mu g/m^3$ LFS PM_{10} (low; daily equivalent), or 100 $\mu g/m^3$ LFS PM_{10} (moderate; daily equivalent), AHR was measured in response to increasing concentrations of nebulized methacholine in terms of **(A)** transpulmonary resistance, **(B)** central airway resistance, and **(C)** diffusing capacity of carbon monoxide. Inflammation of the airway was measured in BAL **(D)** total leukocytes, **(E)** macrophages, **(F)** neutrophils, and **(G)** lymphocytes. mRNA expression of **(H)** *Il6*, **(I)** *Cxcl1/KC*, **(J)** *Tnfα*, **(K)** *Il1β*, and **(L)** *Ahr* was measured in

Statistical analysis

All data are representative of at least 2 experimental repeats. Normally distributed data were determined using the Kolmogrov-Smirnov normality test with Dallal-Wilkinson-Lillie for *P* value. Comparisons between 2 groups were performed using unpaired Student *t* tests or a nonparametric Mann-Whitney test as appropriate. Comparisons between multiple groups were performed using 1-way ANOVA with Fisher least significant difference *post hoc* test. AHR data were assessed using 2-way ANOVA with Tukey *post hoc* test. Echocardiography data were analyzed using a paired *t* test. Analyses were performed using GraphPad Prism Version 10 software (GraphPad Software, Boston, Mass).

RESULTS

Characterization of vegetation-specific LFS PM_{10}

To model LFS exposures experienced during real-world Australian landscape fire events, we generated representative vegetation-specific LFS PM_{10} samples from 2 separate fuel sources (fuel source 1 and fuel source 2) and characterized their respective heavy metal and PAH composition. We designed a custom-built enclosed combustion chamber whereby specific vegetations were burned and resultant LFS collected into dry ice supercooled pure water (Fig 1, *A*). Burn temperatures were monitored and adjusted by modulating air flow throughout the burn time (Fig 1, *B*), and PM fraction was collected. Heavy metal analysis of samples from both fuel source 1 and fuel source 2 demonstrated a rich and diverse range of heavy metals including those typically associated with anthropogenic sources (Fig 1, *C*). To assess PAHs in LFS PM_{10}, 16 priority PAHs as identified by the US Environmental Protection Agency were measured in both samples. All PAHs except for benzo[a]pyrene, benzo[g,h,i]perylene, and indeno[1,2,3-cd]pyrene were represented in both samples of LFS PM_{10} solution (Fig 1, *D*). Taken together, we show that both samples of LFS PM_{10} have differing and unique elemental and chemical profiles. Importantly, we demonstrate a novel method for generating vegetation-specific LFS PM_{10} with heavy metal and PAH composition that can be used in models of exposure to produce reproducible outcomes.

LFS PM_{10} airway exposure alters lung function, independent of airway inflammation, and suppresses inflammatory gene expression

To assess the effects of LFS PM_{10} airway exposure on lung physiology and immune responses, mice were treated with short-term (3 days) and long-term (14 days) LFS PM_{10} (fuel source 1) at 2 different daily equivalent concentrations (low [25 $\mu g/m^3$] or moderate [100$\mu g/m^3$]) (Fig E1, *A* and *B*) or PBS control, and lung function, airway inflammation, and proinflammatory gene expression were measured.[23]

Short-term LFS PM_{10} airway exposure increased methacholine-induced AHR regardless of concentration (control vs 25 $\mu g/m^3$ vs 100 $\mu g/m^3$; 1.41 ± 0.25 vs 1.80 ± 0.49 vs 1.68 ± 0.41) (Fig 2, *A* and *B*), did not affect diffusing capacity of the lungs (Fig 2, *C*), and had minimal effect on airway inflammation with a small but significant increase in macrophages in the short-term low concentration (control vs 25 $\mu g/m^3$; 0.77 ± 0.08 vs 1.28 ± 0.18) (Fig 2, *D-G*). There were no changes to lung structure or function at baseline, as measured by alveolar diameter, collagen deposition around the small airway, or lung function (Fig E2, *A-D* and *G*). However, proinflammatory genes *Il6*, *Cxcl1/KC*, *Tnfα*, and *Ahr* were reduced with short-term LFS PM_{10} airway exposure (Fig 2, *H-J* and *L*), and *Il6* and *Cxcl1/KC* were reduced with long-term LFS PM_{10} airway exposure (Fig 3, *G-H*), whereas *Il1β*, *Muc5ac*, and *Tgfβ* were unaltered with both regimens (Fig 2, *K*; Fig E2, *E* and *F*, in the Online Repository at www.jacionline.org). These reductions were concomitant with no changes in CXCL1/KC, TNF-α, and IL-1β and an increase in IL-6 protein with short-term LFS PM_{10} airway exposure in BAL (Fig 2, *M-P*). We observed similar effects with long-term LFS PM_{10} airway exposure (Fig 3; Fig E3, *A-G*, in the Online Repository at www.jacionline.org) at both concentrations with the exception of a decrease in DF_{CO} (control vs 25 $\mu g/m^3$ vs 100 $\mu g/m^3$; 1.667 × 10^{-9} ± 0.36 vs −2.84 ± 0.90 vs −2.86 ± 0.33) (Fig 3, *C*) and an increase in neutrophils with moderate LFS PM_{10} airway exposure (Fig 3, *F*). While we show that LFS PM generated from fuel source 1 and fuel source 2 has differing elemental and chemical compositions (Fig 1, *B* and *C*), LFS PM_{10} airway exposure from fuel source 2 results in comparable increases in AHR as fuel source 1 (Fig 2; Fig E3). Importantly, LFS PM_{10} generated from fuel source 2, similar to LFS PM_{10} from fuel source 1, did not have any effect on inflammatory cell numbers in BAL. Taken together, these data indicate that LFS PM_{10} airway exposure impairs lung function independent of an overt proinflammatory response or structural changes in the lung. Furthermore, we show that LFS PM_{10} with differing physicochemical profiles have very similar effects on AHR without inducing airway inflammatory cell infiltration. Given the similar effects of LFS PM_{10} from fuel source 1 and fuel source 2 on airway physiology without affecting inflammatory processes, all data presented hereon has been generated using exposure to LFS PM_{10} from fuel source 1 only.

LFS PM_{10} airway exposure induces AHR in small airways and is inhibited when calcium oscillations are abolished

To explore the mechanisms of AHR following LFS PM_{10} airway exposure, mice were treated with short-term/moderate LFS PM_{10} with and without DEX (Fig E1, *C*), and methacholine-induced AHR was assessed in precision cut lung slices (PCLS). Separate PCLS were treated with caffeine/ryanodine to abolish calcium oscillations (Fig 4, *B* and *C*).[21] Grouped analysis of the methacholine concentration response curves demonstrated that the increased AHR observed with LFS PM_{10} airway exposure (sham vs 100 $\mu g/m^3$ LFS; 39.54 ± 9.13 vs 75.84 ± 8.68) was reduced with caffeine/ryanodine treatment to levels of contraction seen in control PCLS (100 $\mu g/m^3$ LFS

whole lung homogenate, and **(M)** IL-6, **(N)** CXCL1/KC, **(O)** TNF-α, and **(P)** IL-1β protein expression was measured in BAL fluid. **(Q)** Mean alveolar diameter was assessed with **(R)** representative photomicrographs (scale bar, 200 μm) showing inflammatory cells near airway and surrounding parenchyma. Two-way ANOVA was performed for *(A* and *B)*. Unpaired *t* tests were performed on LFS PM_{10} groups compared with controls for (*C-Q*). n = 5-13/group. Data presented as mean ± SEM. **P* < .05, ***P* < .01, ****P* < .001, *****P* < .0001.

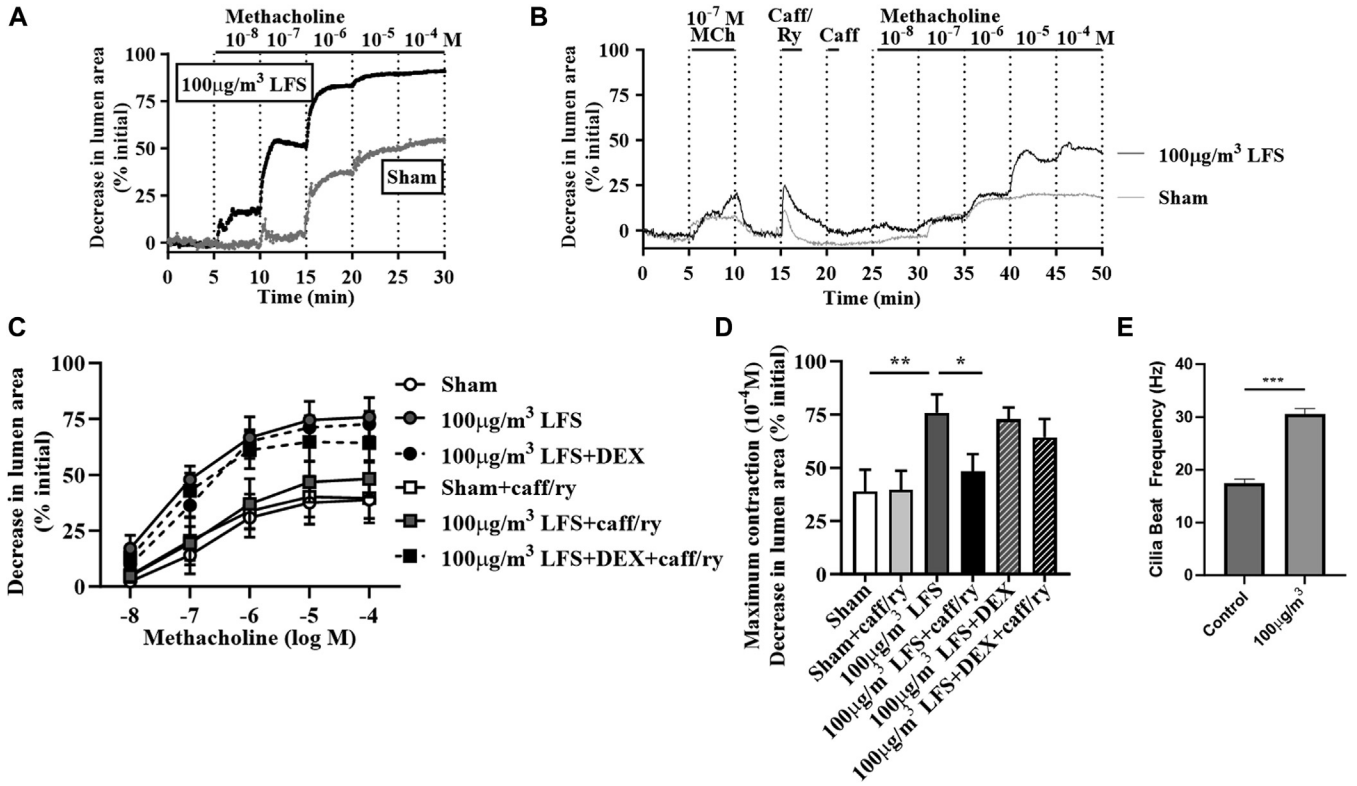

FIG 4. LFS PM_{10} airway exposure induces AHR in small airway and is inhibited when calcium oscillations are abolished. PCLS were prepared from PBS control or short-term/moderate LFS PM_{10} mice with or without DEX and airway visualized by phase-contrast microscopy. **(A** and **B)** Representative frame-by-frame analysis (0.5 Hz) of changes in lumen area with time in the presence of methacholine and/or caffeine (20 mM)/ryanodine (50 μM). **(C)** Grouped analysis determined by averaging the last 30 frames of each concentration of methacholine. **(D)** Maximum contraction to methacholine. **(E)** Cilia beat frequency. n = 3-4/group. $*P < .05$. $**P < .01$. $***P < .001$. *Caff*, Caffeine; *MCh*, methacholine; *Ry*, ryanodine.

vs 100 μg/m^3 LFS+ caffeine/ryanodine; 75.84 ± 8.68 vs 48.25 ± 8.22) (Fig 4, *D* and *E*). Furthermore, DEX treatment did not have an effect on airway contraction. Cilia beat frequency was significantly increased following LFS PM_{10} airway exposure compared with controls (Fig 4, *F*). Together, these data demonstrate that increased AHR following LFS PM_{10} airway exposure is in part caused by changes in calcium oscillations within airway smooth muscle and may explain the inflammation- and structural-independent effects observed *in vivo*.

LFS PM_{10} airway exposure promotes severe, steroid-insensitive disease in a model of mild experimental asthma

AHR is a hallmark feature of asthma, and patients with asthma are disproportionately affected by exposure to LFS.[2,24] Therefore, we next assessed 2 different LFS PM_{10} airway exposure regimens, short-term/moderate (3 days at 100 μg/m^3 daily equivalent) and long-term/low (14 days at 25 μg/m^3 daily equivalent), in experimental asthma (Fig E1, *D*). LFS PM_{10} airway exposure induced AHR in the absence of asthma and increased AHR in the presence of asthma (Fig 5, *A* and *B*). Importantly, DEX treatment reduced OVA-induced AHR of the central airway (OVA vs OVA/DEX; 64.9 ± 30.8 vs 17.2 ± 10.6) and long-term, low LFS PM_{10} OVA–induced AHR (OVA 25 μg/m^3 vs OVA/DEX 25 μg/m^3; 80.8 ± 47.0 vs 25.9 ± 9.3); however, it did not fully reverse short-term/moderate LFS PM_{10}–induced AHR in the presence of asthma (OVA 100 μg/m^3 vs OVA/DEX 100 μg/m^3; 84.1 ± 49.3 vs 55.7 ± 31.5) (Fig 5, *A* and *B*).

Experimental asthma increased total leukocytes, macrophages, eosinophils, and neutrophils (Fig 5, *C-F*), and short-term/moderate LFS PM_{10} airway exposure increased macrophages (OVA vs OVA 100 μg/m^3; 0.49 ± 0.140 vs 0.84 ± 0.191) (Fig 5, *D*). Long-term low, but not short-term moderate, LFS PM_{10} airway exposure decreased eosinophils (OVA vs OVA 25 μg/m^3 vs OVA 100 μg/m^3; 0.09 ± 0.008 vs 0.05 ± 0.010 vs 0.07 ± 0.011) (Fig 5, *F*) in experimental asthma. DEX treatment in the absence or presence of asthma and/or LFS PM_{10} reduced inflammation (total leukocytes, macrophages, eosinophils, and neutrophils) to saline control levels (Fig 5, *C-H*), indicating that these models have steroid-sensitive airway inflammation and suggesting an inflammation-independent, steroid-insensitive mechanism contributing to AHR *in vivo*.

LFS PM_{10} airway exposure with both regimens suppressed expression of the type 2 cytokines *Il4* and *Il13* in lungs, and their expression was affected by DEX treatment in control, but not LFS PM_{10}, groups (Fig 5, *G* and *H*).

LFS PM_{10} airway exposure impairs cardiac function and alters cardiac gene changes involved in remodeling and oxidative stress

LFS exposure is associated with increased adverse cardiovascular events[25,26]; however, the physiologic manifestations of LFS airway exposure on the cardiovascular system are not well

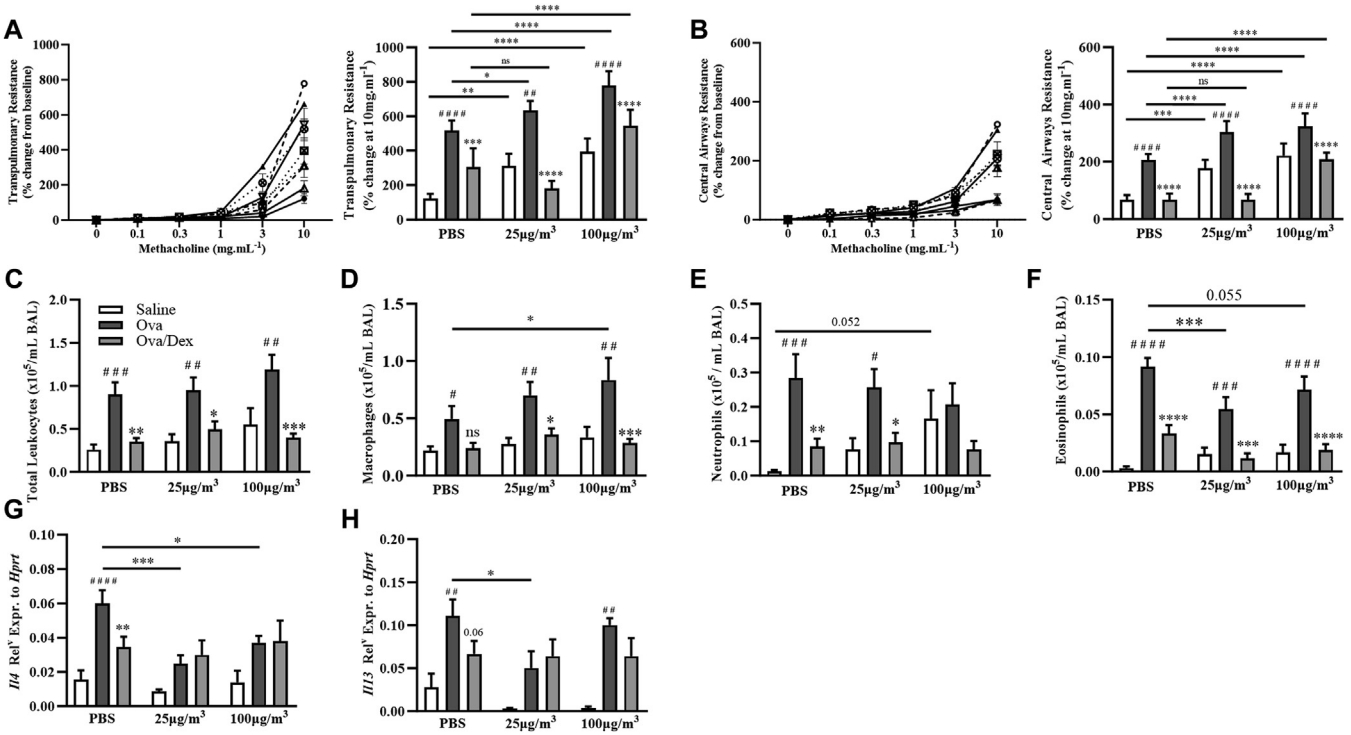

FIG 5. LFS PM_{10} airway exposure increases AHR in experimental asthma independently of an inflammatory profile and causes partial steroid insensitivity. AHR was assessed in terms of **(A)** transpulmonary resistance and **(B)** central airway resistance in response to increasing doses of nebulized methacholine and represented at the maximal dose (10 mg/mL) as a histogram. BAL was assessed in terms of **(C)** total leukocytes, **(D)** macrophages, **(E)** eosinophils, **(F)** neutrophils. mRNA expression was assessed in whole lung homogenate **(G)** *Il4* and **(H)** *Il13*. n = 3-6/group. Data presented as mean ± SEM. **P* < .05, ***P* < .01, ****P* < .001, *****P* < .0001. *Significant compared with OVA in same exposure cluster. #*P* < .05, ##*P* < .01, ###*P* < .001, ####*P* < .0001. #Significant compared with saline in same exposure cluster. *ns,* Not significant.

understood. Therefore, we assessed cardiac function before and after short-term/moderate LFS PM_{10} airway exposure (Fig E1, *E*). Short-term/moderate LFS PM_{10} airway exposure reduced systolic function as measured by LV ejection fraction (Fig 6, *A*). There was also a trend toward a reduction in fractional shortening following LFS PM_{10} airway exposure (Fig 6, *B*) and reduced LV total wall thickness (Fig 6, *C*). Furthermore, *Nppa* expression was increased, and *Myh7* was decreased, following short-term/low and short-term/moderate LFS PM_{10} airway exposure (Fig 6, *D* and *E*). Furthermore, antioxidant genes *Cat*, *Sod1*, and *Sod2* were reduced following short-term/moderate LFS PM_{10} airway exposure (Fig 6, *F-H*), and proinflammatory markers *Il6*, *Tnfα*, and *Il1β* were unchanged in whole heart tissues (Fig 6, *I-K*). In submerged culture of human cardiomyocytes, LFS PM_{10} suspended in culture medium resulted in decreased cell viability in a dose-dependent manner (Fig 6, *L*). Taken together, these results show that LFS PM_{10} airway exposure can reduce LV systolic function and demonstrate a direct effect of LFS PM_{10} airway exposure on cardiac function.

DISCUSSION

Here, we have developed a platform for the generation of physiologically relevant vegetation-specific LFS PM and assessed its effects on respiratory and cardiovascular outcomes. We demonstrate that short- or long-term, low- or moderate-airway exposure to LFS PM_{10}, in the absence or presence of asthma, can have detrimental effects on lung function, altering inflammatory profiles in the heart and lung and impairing cardiovascular functions.

Our approach to collecting highly representative LFS PM_{10} was to burn vegetation from plant and tree species endemic to the southeastern region of Australia to provide a vegetation- and/or geography-specific sample for analysis. Our novel platform for the generation of vegetation-specific LFS PM into liquid solution allowed safe, and consistent LFS PM generation, with composition relevant to a real-world landscape fire event, including the presence of heavy metals and PAHs.[7,27-29] Importantly, heavy metals are negatively associated with lung function,[30,31] and the variation in the abundance of these elements in real-world LFS is likely due to the proximity of vegetation to anthropogenic sources of pollution.[27-29] Furthermore, the presence of PAHs is consistent with the incomplete combustion of organic material such as fossil fuels, coal, plastics, and landscape biomatter.[32] While there is limited real-world air quality PAH data generated during landscape fire events, it will be important in future studies to monitor these, as PAHs are known to have detrimental effects on respiratory and cardiovascular outcomes.[7,33,34]

Models are required to understand the mechanisms that underpin the physiologic effects of LFS PM_{10} airway exposure on lungs and heart. During landscape fire events, the durations and concentrations of exposure vary significantly[23]; therefore, we focused on modeling exposures in the Hunter Valley and

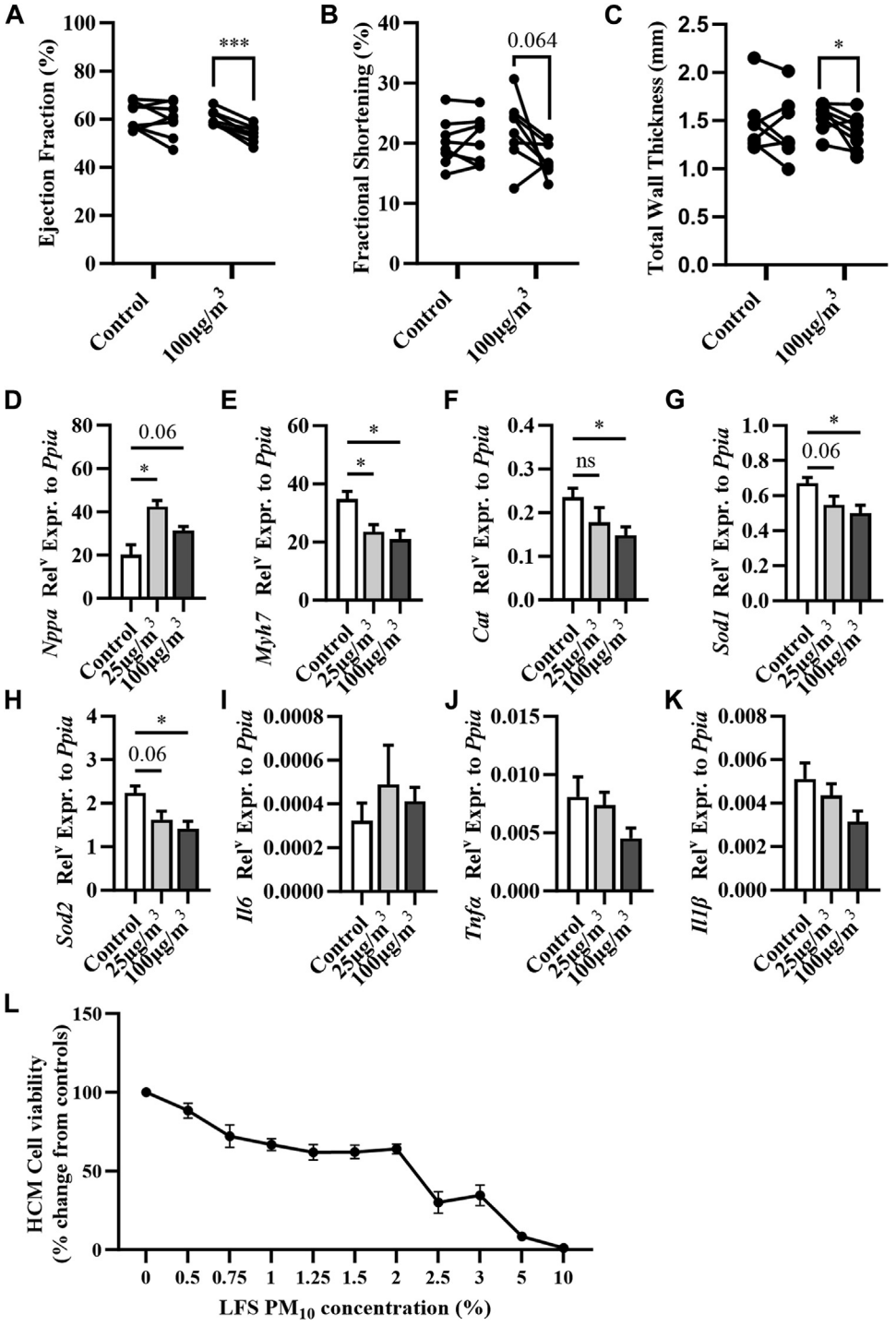

FIG 6. Short-term LFS PM_{10} airway exposure impairs cardiac function and alters cardiac-associated and oxidative stress–associated gene expression. Mouse echocardiography was used to assess **(A)** LV ejection fraction, **(B)** fractional shortening, and **(C)** total wall thickness in mice following short-term (3 days) airway exposure to PBS (control) or 100 $\mu g/m^3$ LFS PM_{10} daily equivalent. mRNA expression of **(D)** *Nppa*, **(E)** *Myh7*, **(F)** *Cat*, **(G)** *Sod1*, **(H)** *Sod2*, **(I)** *Il6*, **(J)** *Tnfα*, and **(K)** *Il1β* in cardiac homogenates from mice administered intranasally with PBS (control), 25 $\mu g/m^3$ LFS PM_{10} daily equivalent, or 100 $\mu g/m^3$ LFS PM_{10} daily equivalent for 3 days. **(L)** Human cardiomyocyte cell viability in response to increasing concentrations of LFS PM_{10} after 72 hours. Paired *t* tests were performed for *(A-C)* (before vs after LFS PM_{10} airway exposure). For *(D-K)*, unpaired *t* tests were performed (PBS vs 25 $\mu g/m^3$ or 100 $\mu g/m^3$ LFS PM_{10}). n = 8/group. Data presented as mean ± SEM. $^*P < .05$, $^{***}P < .001$. *ns,* Not significant.

Newcastle region, which experienced low to moderate LFS PM_{10} levels compared with other parts of the state during the 2019-2020 period. We show that exposure of the airway to LFS PM_{10} (low or moderate, short-term or long-term, and/or 2 different types of LFS PM_{10}) induces increased AHR to a similar magnitude. Importantly, while we show that LFS PM from fuel source 1 and fuel source 2 have differing elemental and chemical composition, inhalation of LFS PM_{10} from both fuel sources produces nearly identical pathophysiologic outcomes. Therefore, our data suggest that while the physicochemical properties of LFS PM may vary for different fires and locations, the pathophysiologic effects produced in the lungs may be similar.

Interestingly, we show that that LFS PM_{10}–induced increased AHR is independent of overt inflammatory processes in the lungs or airway or structural changes in the lungs. We show decreased *Il6* and *Cxcl1/KC* gene expression in lung homogenates concomitant with no changes in protein levels in the BAL fluid, highlighting a potential disconnect between gene and protein expression and inflammatory cell recruitment following airway exposure to LFS PM_{10}. PM derived from different sources varies in terms of chemical and elemental composition, which likely explains the disconnect between inflammation profiles in our models compared with previous studies.[6,7] Nevertheless, and in support of our findings, AHR can exist in the absence of a proinflammatory profile and has been attributed to epithelial dysfunction, altered expression of contractile proteins (increased ratio of F-actin to G-actin), and changes in myosin isoforms and/or myosin light chain kinases.[19,35-39] Whether these are altered in our models and contribute to AHR is yet to be determined, but may provide important avenues for future therapeutic targets.

Calcium signaling pathways associated with smooth muscle contraction have been shown to be affected by respiratory stimuli, such as OVA and cigarette smoke.[19,40,41] In the absence of a robust inflammatory profile and structural changes that are typically associated with AHR, we next assessed the role of calcium signaling pathways in PCLS from LFS PM_{10} mice. Interestingly, we show that the effects of increased contractility to methacholine *in vivo* are maintained in PCLS obtained from LFS PM_{10} mice, suggesting that LFS PM_{10} airway exposure induces changes to airway smooth muscle and not changes in lung structure. In untreated PCLS, methacholine contraction has been shown to be associated with increases in calcium oscillations and sensitivity.[21] To assess the contribution of calcium sensitivity to altered contraction following LFS PM_{10} airway exposure, we measured reactivity to methacholine in PCLS treated with caffeine and ryanodine to empty the intracellular calcium stores and lock ryanodine receptors in an open state.[41] Similar to previous studies, caffeine/ryanodine treatment had no effect on the potency or maximum contraction to methacholine in PCLS from control mice.[41] However, in PCLS from LFS PM_{10} mice, contraction to methacholine was reduced following caffeine/ryanodine treatment, suggesting that the increased contraction to methacholine following LFS PM_{10} airway exposure is, in part, driven by calcium oscillations. Calcium oscillations in airway smooth muscle are primarily mediated through inositol trisphosphate and ryanodine receptors[42-44]; however, whether levels of these receptors in the airway are altered following LFS exposure remains to be determined and may also provide additional avenues for future therapeutic targets. While the direct mechanisms of how LFS PM_{10} alters calcium oscillations remain to be fully elucidated, it is possible that LFS PM_{10} could be binding to calcium channels (eg, IP3R, RyR, SERCA) on the sarcoplasmic reticulum and altering opening time/calcium release in the presence of a stimulus such as methacholine. Cigarette smoke extract–treated human airway smooth muscle cells can enhance store-operated Ca^{2+} entry and increased expression of Orai1 and STIM1,[45] which may be another possible mechanism of LFS-induced AHR. Together, our PCLS and *in vivo* data show that LFS alone can increase AHR due to changes in calcium oscillation pathways and independent of inflammation. Furthermore, in LFS+DEX–treated mice, AHR is likely due to changes in both calcium oscillation and calcium sensitivity signaling pathways. To our knowledge, no studies to date have assessed DEX treatment on calcium sensitivity pathways in airway smooth muscle; however, DEX has been shown to increase RhoA/Rho-associated kinase pathways in Schlemm canal endothelial cells and protein kinase C in brain tissue, highlighting the possibility that DEX increases calcium sensitivity pathways.[46,47] Further studies using specific airway smooth muscle–targeted knockdown of components of the calcium oscillation and signaling pathways to decipher the roles of LFS in the absence and presence of DEX are warranted.

Our data also uncovered a decrease in gas exchange following long-term (14 days) low- and moderate-concentration LFS PM_{10} airway exposure, which has important health ramifications, especially for individuals with preexisting conditions and may explain the increase in emergency department presentations and hospitalization admissions for respiratory conditions such as asthma[3] and cardiovascular conditions such as myocardial infarctions, heart failure, and arrhythmias during the landscape fire season.[48,49] We observed this impaired lung function independent of changes in alveolar size, suggesting that long-term airway exposure to LFS PM_{10} (regardless of concentration) can impair gas exchange at the functional level preceding the onset of emphysema-like alveolar destruction.[12]

AHR is an important hallmark feature of asthma, and patients with asthma are disproportionately affected by LFS compared with individuals without asthma.[2,4] We show that LFS PM_{10} airway exposure in experimental asthma changes the phenotype and severity of asthma and results in a non–type 2 dominant, steroid-insensitive model of asthma with increased AHR. This has important ramifications for patients with asthma, as it suggests that prescribed corticosteroid medication may be inefficient at controlling underlying inflammation and disease symptoms and may need to be increased, or new therapies, management strategies, and avoidance strategies may need to be identified and applied during landscape fire events.

Pollution from landscape fires is associated with increased cardiac-associated emergency department presentations and admissions[3]; however, the direct effects and mechanisms underlying this association are less well understood. In our study, mice with short-term/moderate LFS PM_{10} airway exposure exhibited impaired cardiac function, as seen by a decrease in LV ejection fraction (approximately 10% from baseline), fractional shortening ($P = .064$), and concomitant thinning of cardiac walls. These findings are consistent with previous human studies[50-53] and animal models of air pollution–induced cardiovascular diseases.[54-56] While we show decreased cell viability in HCMs exposed to LFS PM_{10}, the underlying mechanism is not fully understood, and the activation of aryl hydrocarbon receptor by PAHs and other organic compounds inherent to real-world PM is a likely cause. PAHs induce reactive oxygen species production, increased matrix metalloproteinase activity, and actin reorganization in rat aortic vascular

smooth muscle cells.[57] Furthermore, a short-term exposure (48 hours) to $PM_{2.5}$ caused an increase in oxidative stress, dysregulated conduction activity, and beat period irregularity in cardiomyocytes derived from human inducible pluripotent stem cells.[58] Interestingly, diesel-derived $PM_{2.5}$ exposure increased reactive oxygen species production and led to suppression of Ca^{2+} homeostasis and disintegration of mitochondrial cristae in HL-1 mouse cardiomyocyte cell lines.[59]

Our findings agree with those of others who have shown that LFS causes lung function decline in adult nonhuman primates exposed in early life and that LFS PM may result in a suppression in inflammatory processes.[60,61] Specifically, in the study by Black et al,[61] rhesus macaque monkeys were exposed to wildfire smoke in early life. At 3 years of age, wildfire smoke–exposed monkeys displayed significantly reduced lung function per unit of body weight relative to control animals, and PBMCs collected from wildfire-exposed animals had a reduced ability to respond to LPS-induced inflammatory events.[61] Furthermore, in the study by Hamon et al,[60] THP-1 monocytic cells were exposed to LFS particulates (submerged) resulting in decreased IP-10, MCP-1, MIP-1α and MIP-1β protein along with decreased phagocytic and efferocytic function.

Our observed LFS PM_{10}–induced cardiomyopathy-like phenotype was also associated with increased *Nppa* and reduced *Myh7*. NPPA is released by cardiomyocytes in response to cardiac stress events and is an important biomarker for congenital heart defects,[62] and myocardial chamber differentiation and mutations in *Myh7* are associated with structural abnormalities of cardiac muscle that can lead to cardiomyopathy.[63] In addition, we show a significant reduction of the critical endogenous antioxidants *Sod1*, *Sod2*, and *Cat* in response to LFS PM_{10} airway exposure, suggesting that oxidative stress may be contributing to features of cardiomyopathy.[64]

Our study is the first to show a causal link between LFS PM_{10} airway exposure and cardiac dysfunction, and, importantly, our findings were observed after only 3 days of daily LFS PM_{10} airway exposure. Future studies assessing the effects of long-term LFS PM_{10} airway exposure on cardiac function and in the presence of existing cardiovascular and metabolic diseases are warranted.

Our pipeline provides for vegetation-specific LFS PM_{10} generation and allows for assessing the effects that LFS PM_{10} has on mouse models of short- and long-term, low- and moderate-concentration airway exposure in a reproducible manner. Given the reproducibility of results following exposures, this model can be used as a platform for assessing mechanisms following exposure to LFS PM from different fuel sources and geographical locations and testing novel therapies. Importantly, our platform can be adapted to model different fuel loads and sources, types of vegetation, and burn conditions in a geography-specific manner and inform how different levels of LFS airway exposure affect the lung and heart. We have focused on LFS PM_{10} effects on respiratory and cardiovascular outcomes in this study; however, based on our findings, we anticipate additional systemic effects in the gastrointestinal tract and brain following LFS PM_{10} airway exposure, which provide additional future avenues of research beyond the scope of our study. Our data also suggest that targeting airway smooth muscle and/or oxidative stress pathways may provide novel strategies for the prevention and/or treatment of respiratory and/or cardiovascular disease following inhalation of LFS PM_{10} following landscape fire events.

DISCLOSURE STATEMENT

This study was funded by Medical Research Future Fund Emerging Priorities and Consumer-Driven Research Initiative Bushfire Impact Research Grant, Heart Foundation Vanguard Grant, and Heart Foundation Future Leader Fellowship to D.T.M.N.

Disclosure of potential conflict of interest: The authors declare that they have no relevant conflicts of interest.

Key messages

- **The authors developed a highly representative platform for investigating the mechanisms that underpin landscape fire PM inhalation on respiratory and cardiovascular disease outcomes.**
- **Inhalation results in AHR and steroid insensitivity in experimental asthma that are independent of significant changes in airway inflammation as well as decreased cardiac function.**
- **These data suggest that targeting airway smooth muscle and/or oxidative stress pathways may provide novel strategies for the prevention and/or treatment of respiratory and/or cardiovascular disease landscape fire PM.**

REFERENCES

1. United Nations Environment Programme & GRID-Arendal. Spreading like Wildfire: The Rising Threat of Extraordinary Landscape Fires—A UNEP Rapid Response Assessment. Nairobi; 2022.
2. Goldman M, FLynn A, Cartwright A, Bell R, Sharon D, Bui D, et al. Bushfire Smoke Impact Survey 2019-2020. 2020 Bushfire Smoke: Are you coping? Asthma Australia; 2020.
3. Walter CM, Schneider-Futschik EK, Knibbs LD, Irving LB. Health impacts of bushfire smoke exposure in Australia. Respirology 2020;25:495-501.
4. Beyene T, Harvey ES, Van Buskirk J, McDonald VM, Jensen ME, Horvat JC, et al. 'Breathing fire': impact of prolonged bushfire smoke exposure in people with severe asthma. Int J Environ Res Public Health 2022;19:7419.
5. Bui D, Davis S, Flynn A, Bell R, Dharmage S. Impact of recent catastrophic bushfires on people with asthma in Australia: health, social and financial burdens. Respirology 2021;26:296-7.
6. Isley CF, Taylor MP. Atmospheric remobilization of natural and anthropogenic contaminants during wildfires. Environ Pollut 2020;267:115400.
7. Ghetu CC, Rohlman D, Smith BW, Scott RP, Adams KA, Hoffman PD, et al. Wildfire impact on indoor and outdoor PAH air quality. Environ Sci Technol 2022;56:10042-52.
8. Essilfie AT, Horvat JC, Kim RY, Mayall JR, Pinkerton JW, Beckett EL, et al. Macrolide therapy suppresses key features of experimental steroid-sensitive and steroid-insensitive asthma. Thorax 2015;70:458-67.
9. Kim RY, Horvat JC, Pinkerton JW, Starkey MR, Essilfie AT, Mayall JR, et al. MicroRNA-21 drives severe, steroid-insensitive experimental asthma by amplifying phosphoinositide 3-kinase-mediated suppression of histone deacetylase 2. J Allergy Clin Immunol 2017;139:519-32.
10. Kim RY, Pinkerton JW, Essilfie AT, Robertson AAB, Baines KJ, Brown AC, et al. Role for NLRP3 inflammasome-mediated, IL-1beta-dependent responses in severe, steroid-resistant asthma. Am J Respir Crit Care Med 2017;196:283-97.
11. Pinkerton JW, Kim RY, Brown AC, Rae BE, Donovan C, Mayall JR, et al. Relationship between type 2 cytokine and inflammasome responses in obesity-associated asthma. J Allergy Clin Immunol 2022;149:1270-80.
12. Fricker M, Goggins BJ, Mateer S, Jones B, Kim RY, Gellatly SL, et al. Chronic cigarette smoke exposure induces systemic hypoxia that drives intestinal dysfunction. JCI Insight 2018;3:e94040.
13. Ali MK, Kim RY, Brown AC, Donovan C, Vanka KS, Mayall JR, et al. Critical role for iron accumulation in the pathogenesis of fibrotic lung disease. J Pathol 2020;251:49-62.
14. Tu X, Kim RY, Brown AC, de Jong E, Jones-Freeman B, Ali MK, et al. Airway and parenchymal transcriptomics in a novel model of asthma and COPD overlap. J Allergy Clin Immunol 2022;150:817-29.e6.

15. Gomez HM, Pillar AL, Brown AC, Kim RY, Ali MK, Essilfie AT, et al. Investigating the links between lower iron status in pregnancy and respiratory disease in offspring using murine models. Nutrients 2021;13:4461.
16. Tu X, Gomez HM, Kim RY, Brown AC, de Jong E, Galvao I, et al. Airway and parenchyma transcriptomics in a house dust mite model of experimental asthma. Respir Res 2023;24:32.
17. Kim RY, Sunkara KP, Bracke KR, Jarnicki AG, Donovan C, Hsu AC, et al. A microRNA-21-mediated SATB1/S100A9/NF-kappaB axis promotes chronic obstructive pulmonary disease pathogenesis. Sci Transl Med 2021;13:eaav7223.
18. Sverdlov AL, Elezaby A, Qin F, Behring JB, Luptak I, Calamaras TD, et al. Mitochondrial reactive oxygen species mediate cardiac structural, functional, and mitochondrial consequences of diet-induced metabolic heart disease. J Am Heart Assoc 2016;5:e002555.
19. Donovan C, Royce SG, Esposito J, Tran J, Ibrahim ZA, Tang ML, et al. Differential effects of allergen challenge on large and small airway reactivity in mice. PLoS One 2013;8:e74101.
20. Donovan C, Simoons M, Esposito J, Ni Cheong J, Fitzpatrick M, Bourke JE. Rosiglitazone is a superior bronchodilator compared to chloroquine and beta-adrenoceptor agonists in mouse lung slices. Respir Res 2014;15:29.
21. Bourke JE, Bai Y, Donovan C, Esposito JG, Tan X, Sanderson MJ. Novel small airway bronchodilator responses to rosiglitazone in mouse lung slices. Am J Respir Cell Mol Biol 2014;50:748-56.
22. Donovan C, Kim RY, Galvao I, Jarnicki AG, Brown AC, Jones-Freeman B, et al. Aim2 suppresses cigarette smoke-induced neutrophil recruitment, neutrophil caspase-1 activation and anti-Ly6G-mediated neutrophil depletion. Immunol Cell Biol 2022;100:235-49.
23. Data download facility: regional air quality. NSW Government Department of Planning and Environment. Available at: https://www.dpie.nsw.gov.au/air-quality/air-quality-data-services/data-download-facility. Accessed May 24, 2020.
24. Dennekamp M, Abramson MJ. The effects of bushfire smoke on respiratory health. Respirology 2011;16:198-209.
25. Lankaputhra M, Johnston FH, Otahal P, Jalil E, Dennekamp M, Negishi K. Cardiac autonomic impacts of bushfire smoke—a prospective panel study. Heart Lung Circ 2023;32:52-8.
26. Efraemson D, Colgan J, Greenwood M. The cardiovascular effects of exposure to particulate matter from bushfire smoke in patients with pre-existing cardiovascular disease. Br J Card Nurs 2020;15:1-7.
27. Odigie KO, Flegal AR. Pyrogenic remobilization of historic industrial lead depositions. Environ Sci Technol 2011;45:6290-5.
28. Odigie KO, Flegal AR. Trace metal inventories and lead isotopic composition chronicle a forest fire's remobilization of industrial contaminants deposited in the angeles national forest. PLoS One 2014;9:e107835.
29. Kristensen LJ, Taylor MP, Odigie KO, Hibdon SA, Flegal AR. Lead isotopic compositions of ash sourced from Australian bushfires. Environ Pollut 2014;190:159-65.
30. Zeng H, Dong B, Wang N, Xu W, Guo L, Liu J, et al. The effects of metals and mixture exposure on lung function and the potential mediating effects of oxidative stress. Environ Geochem Health 2022;45:2263-75.
31. Wei W, Wu X, Bai Y, Li G, Feng Y, Meng H, et al. Lead exposure and its interactions with oxidative stress polymorphisms on lung function impairment: results from a longitudinal population-based study. Environ Res 2020;187:109645.
32. Reizer E, Viskolcz B, Fiser B. Formation and growth mechanisms of polycyclic aromatic hydrocarbons: a mini-review. Chemosphere 2022;291:132793.
33. Alhamdow A, Lindh C, Albin M, Gustavsson P, Tinnerberg H, Broberg K. Early markers of cardiovascular disease are associated with occupational exposure to polycyclic aromatic hydrocarbons. Sci Rep 2017;7:9426.
34. Cilluffo G, Ferrante G, Murgia N, Mancini R, Pichini S, Cuffari G, et al. Effects of polycyclic aromatic hydrocarbons on lung function in children with asthma: a mediation analysis. Int J Environ Res Public Health 2022;19:1826.
35. McVicker CG, Leung SY, Kanabar V, Moir LM, Mahn K, Chung KF, et al. Repeated allergen inhalation induces cytoskeletal remodeling in smooth muscle from rat bronchioles. Am J Respir Cell Mol Biol 2007;36:721-7.
36. Moir LM, Leung SY, Eynott PR, McVicker CG, Ward JP, Chung KF, et al. Repeated allergen inhalation induces phenotypic modulation of smooth muscle in bronchioles of sensitized rats. Am J Physiol Lung Cell Mol Physiol 2003;284:L148-59.
37. Yamamoto N, Kan OK, Tatsuta M, Ishii Y, Ogawa T, Shinozaki S, et al. Incense smoke-induced oxidative stress disrupts tight junctions and bronchial epithelial barrier integrity and induces airway hyperresponsiveness in mouse lungs. Sci Rep 2021;11:7222.
38. Witzenrath M, Ahrens B, Schmeck B, Kube SM, Hippenstiel S, Rosseau S, et al. Rho-kinase and contractile apparatus proteins in murine airway hyperresponsiveness. Exp Toxicol Pathol 2008;60:9-15.
39. Bazett M, Haston CK. Airway hyperresponsiveness in FVB/N delta F508 cystic fibrosis transmembrane conductance regulator mice. J Cyst Fibros 2014;13:378-83.
40. Prihandoko R, Kaur D, Wiegman CH, Alvarez-Curto E, Donovan C, Chachi L, et al. Pathophysiological regulation of lung function by the free fatty acid receptor FFA4. Sci Transl Med 2020;12:eaaw9009.
41. Donovan C, Seow HJ, Royce SG, Bourke JE, Vlahos R. Alteration of airway reactivity and reduction of ryanodine receptor expression by cigarette smoke in mice. Am J Respir Cell Mol Biol 2015;53:471-8.
42. Janssen LJ. Ionic mechanisms and Ca2+ regulation in airway smooth muscle contraction: do the data contradict dogma? Am J Physiol Lung Cell Mol Physiol 2002;282:L1161-78.
43. Pabelick CM, Sieck GC, Prakash YS. Invited review: significance of spatial and temporal heterogeneity of calcium transients in smooth muscle. J Appl Physiol (1985) 2001;91:488-96.
44. Bergner A, Sanderson MJ. Acetylcholine-induced calcium signaling and contraction of airway smooth muscle cells in lung slices. J Gen Physiol 2002;119:187-98.
45. Wylam ME, Sathish V, VanOosten SK, Freeman M, Burkholder D, Thompson MA, et al. Mechanisms of cigarette smoke effects on human airway smooth muscle. PLoS One 2015;10:e0128778.
46. Fujimoto T, Inoue T, Kameda T, Kasaoka N, Inoue-Mochita M, Tsuboi N, et al. Involvement of RhoA/Rho-associated kinase signal transduction pathway in dexamethasone-induced alterations in aqueous outflow. Invest Ophthalmol Vis Sci 2012;53:7097-108.
47. Dwivedi Y, Pandey GN. Administration of dexamethasone up-regulates protein kinase C activity and the expression of gamma and epsilon protein kinase C isozymes in the rat brain. J Neurochem 1999;72:380-7.
48. Data update: short-term health impacts of the 2019-20 Australian bushfires. Australian Institute of Health and Welfare; 2021. Available at: https://www.aihw.gov.au/reports/environment-and-health/data-update-health-impacts-2019-20-bushfires/contents/about. Accessed July 25, 2022.
49. Rabe KF, Hurst JR, Suissa S. Cardiovascular disease and COPD: dangerous liaisons? Eur Respir Rev 2018;27:180057.
50. Al-Kindi SG, Brook RD, Biswal S, Rajagopalan S. Environmental determinants of cardiovascular disease: lessons learned from air pollution. Nat Rev Cardiol 2020;17:656-72.
51. Rajagopalan S, Landrigan PJ. Pollution and the heart. N Engl J Med 2021;385:1881-92.
52. de Bont J, Jaganathan S, Dahlquist M, Persson A, Stafoggia M, Ljungman P. Ambient air pollution and cardiovascular diseases: an umbrella review of systematic reviews and meta-analyses. J Intern Med 2022;291:779-800.
53. Ji JS. Air pollution and cardiovascular disease onset: hours, days, or years? Lancet Public Health 2022;7:e890-1.
54. Qin G, Xia J, Zhang Y, Guo L, Chen R, Sang N. Ambient fine particulate matter exposure induces reversible cardiac dysfunction and fibrosis in juvenile and older female mice. Part Fibre Toxicol 2018;15:27.
55. Cui L, Shi L, Li D, Li X, Su X, Chen L, et al. Real-ambient particulate matter exposure-induced cardiotoxicity in C57/B6 Mice. Front Pharmacol 2020;11:199.
56. Jiang J, Li Y, Liang S, Sun B, Shi Y, Xu Q, et al. Combined exposure of fine particulate matter and high-fat diet aggravate the cardiac fibrosis in C57BL/6J mice. J Hazard Mater 2020;391:122203.
57. Ju S, Lim L, Ki YJ, Choi DH, Song H. Oxidative stress generated by polycyclic aromatic hydrocarbons from ambient particulate matter enhance vascular smooth muscle cell migration through MMP upregulation and actin reorganization. Part Fibre Toxicol 2022;19:29.
58. Argenziano M, Yang J, Burgos Angulo M, McDonald TV. Abstract P309: particulate matter increases oxidative stress and shortens the action potential in IPS-derived cardiomyocytes. Circ Res 2021;129:AP309-AP.
59. Shin TH, Kim SG, Ji M, Kwon DH, Hwang JS, George NP, et al. Diesel-derived PM(2.5) induces impairment of cardiac movement followed by mitochondria dysfunction in cardiomyocytes. Front Endocrinol (Lausanne) 2022;13:999475.
60. Hamon R, Tran HB, Roscioli E, Ween M, Jersmann H, Hodge S. Bushfire smoke is pro-inflammatory and suppresses macrophage phagocytic function. Sci Rep 2018;8:13424.
61. Black C, Gerriets JE, Fontaine JH, Harper RW, Kenyon NJ, Tablin F, et al. Early life wildfire smoke exposure is associated with immune dysregulation and lung function decrements in adolescence. Am J Respir Cell Mol Biol 2017;56:657-66.
62. Man J, Barnett P, Christoffels VM. Structure and function of the Nppa-Nppb cluster locus during heart development and disease. Cell Mol Life Sci 2018;75:1435-44.
63. Hesaraki M, Bora U, Pahlavan S, Salehi N, Mousavi SA, Barekat M, et al. A novel missense variant in actin binding domain of MYH7 is associated with left ventricular noncompaction. Front Cardiovasc Med 2022;9:839862.
64. D'Oria R, Schipani R, Leonardini A, Natalicchio A, Perrini S, Cignarelli A, et al. The role of oxidative stress in cardiac disease: from physiological response to injury factor. Oxid Med Cell Longev 2020;2020:5732956.

METHODS

Assessing heavy metal content in LFS PM_{10}

The metal(loid) concentration of LFS PM_{10} concentrate was assessed using ICP-MS as previous described.[E1,E2] Roughly 0.5 g of the sample was weighed in triplicates and digested using a microwave-assisted digestion system (MARS 6; CEM Corp, Matthews, NC) in 5 mL of Aqua Regia (HNO_3 and HCl, 1:3) until a clear solution was formed. The resultant mixture was then diluted to 50 mL using deionized water and passed through a 0.25-μm syringe filter. The filtrate was then used to analyze the metal(loid) concentration using ICP-MS (Agilent 7500ce; Agilent Technologies, Inc, Santa Clara, Calif) coupled with an Octopole Reaction System for multielemental analysis. Commercially available standard metal solutions were used as internal standards to calculate the %recovery.

Assessing abundance of polycyclic aromatic hydrocarbons in LFS PM_{10}

The qualitative and quantitative analysis of PAHs in LFS PM_{10} concentrate was performed using GC-MS. First, the extraction of PAHs from LFS solution was conducted using standard liquid-liquid extraction, where 1 mL of the extract was mixed with 10 mL of analytical grade hexane in closed glass vials and allowed to incubate on a rotary shaker for 20 minutes, the upper solvent layer was carefully removed, and the aqueous layer was further washed with 10 mL of hexane in 3 consecutive steps (10 mL each). Then, the combined extracts (30 mL) were further concentrated to 1 mL in a temperature-controlled water bath operated at 40°C under N_2. The concentrated samples were analyzed twice (separate aliquots) in triplicate using an Agilent 7010A (Agilent Technologies, Inc) triple quadrupole system fitted with a HP-5ms column, under specific operating conditions.

Calculation of human relevant LFS PM_{10} inhalation levels

Air quality measuring data were obtained from the New South Wales Department of Planning and Environment[E3] for several locations along the southeastern coast of Australia. For a period in December 2019, the average daily PM_{10} exposure concentrations were determined to be 25 $\mu g/m^3$ averaged over 14 days and 100 $\mu g/m^3$ averaged over 3 days. We consider these concentrations and durations of exposure to be representative of those experienced at various locations throughout the state.

Daily human PM_{10} exposure was determined for an average Australian woman by multiplying the aforementioned daily PM_{10} inhalation concentrations of either 25 $\mu g/m^3$ (0.025 μg/L) or 100 $\mu g/m^3$ (0.1 μg/L) and total tidal volume (L/day). Total tidal volume (L/day) was calculated by multiplying the average tidal volume value of 8 mL/kg/breath (0.008 L/kg/breath),[E4] the average weight of an Australian woman of 71.1 kg,[E5] average breathing rate (20 breaths/minute), and 1440 minutes/day. Daily human (71.1 kg) PM_{10} inhalation concentrations were normalized to mouse (0.02 kg) equivalent doses based on weight to determine representative human-relevant, mouse-normalized concentrations for LFS PM_{10} exposure models.

Alveolar enlargement

Formalin-fixed paraffin-embedded lungs were sectioned (5 μm) and stained with hemoxylin and eosin. A minimum of 10 random parenchymal images (no airway or blood vessels present) were overlayed with 11 lines, and mean linear intercept counts or point counts for destructive index were conducted as previously described.

Collagen deposition around small airway

Collagen surrounding small airway was assessed using Sirius Red/Fast Green counterstained lung sections, whereby 6 light micrographs of small airway taken at 40× magnification were randomly selected per mouse, and total collagen area was manually outlined and calculated per μm of basement membrane length using ImageJ software version 1.52a (National Institutes of Health, Bethesda, Md).

Airway contractility

Following 3 days of inhalation of LFS PM_{10} or PBS (control), mice were euthanized on day 4. PCLS were prepared as previously described.[E6-E10] Briefly, trachea were cannulated and lungs inflated with 2% low melting point agarose (Invitrogen, Life Technologies, Scoresby, Victoria, Australia) in sterile Hanks' Balanced Salt Solution (sHBSS; Life Technologies) supplemented with 40 mM HEPES. Lungs were cooled (20 minutes, 4°C) to solidify the agarose, and sections were cut (150 μm) using a Compresstome vibrating microtome (Precisionary Instruments, Greenville, NC) and incubated overnight in Dulbecco modified Eagle medium supplemented with 1% penicillin-streptomycin (37°C, 5% CO_2). Each PCLS was mounted in a custom-built perfusion chamber and perfused with sHBSS and with increasing concentrations of methacholine (0.1-100 μM in sHBSS). Separate PCLS were exposed to caffeine (20 mM; Sigma-Aldrich) and ryanodine (50 mM; Sigma-Aldrich) to clamp intracellular calcium ([Ca21]i) at a sustained high level as previously described.[E11] Before treatment with increasing concentrations of methacholine (0.1-100 μM in sHBSS), digital images of airway (180-300 μm in diameter) were recorded in time lapse (0.5 Hz) using a phase contrast inverted microscope (Eclipse Ti-U; Nikon Instruments, Melville, NY) with a charge-coupled device camera (TM-62EX Pulnix; Adept Turnkey, Brookvale, New South Wales, Australia). Images were then analyzed using image acquisition software (Video Savant; IO Industries, Inc, London, Ontario, Canada). Airway lumen area in each image was calculated by pixel summation by defining a grayscale threshold. Data are presented as mean ± SEM and normalized to the initial airway lumen area. Cilia beat frequencies were measured using 600 images recorded at 300 frames per second as previously described.[E12] Changes in the gray intensity of the image that result from cilia movement were analyzed by selecting a line scan of 3 pixels and counting the number of oscillations over the 2-second recording. Cilia beat frequencies (Hz) were calculated by dividing the number of oscillations/second. Data are presented as mean ± SEM.

Primary human cardiomyocyte cultures

Primary Human Cardiac Myocytes (HCM) were purchased from PromoCell (Heidelberg, Germany) and cultured according to manufacturer's instructions using PromoCell Myocyte growth media (5% [vol/vol] fetal calf serum, 0.5 ng/mL recombinant human epidermal growth factor, 2 ng/mL recombinant human basic fibroblast growth factor, 5 μg/mL recombinant human

insulin) supplemented with 1% (vol/vol) Penicillin-Streptomycin [Sigma-Aldrich]). Briefly, 1×10^6 HCM were seeded and grown in Corning T75 flasks (Sigma-Aldrich) in an incubator at 37°C under 5% CO_2 conditions. At 80% to 90% confluency, HCM were gently detached using the DetachKit (PromoCell), collected into Corning 50-mL centrifuge tubes (Sigma-Aldrich), and centrifuged at 300*g* for 10 minutes at room temperature. The resulting supernatant were discarded, and the HCM pellet was resuspended with 5 to 10 mL of prewarmed Myocyte Growth Medium (PromoCell, Heidelberg, Germany). Total viable cells were enumerated with Invitrogen Countess Automated Cell Counter (Thermo Fisher Scientific, New South Wales, Australia) and 1×10^5 live HCM were seeded in triplicate into Corning 96-well white polystyrene microplate (Sigma-Aldrich). Seeded HCM were incubated in an incubator at 37°C under 5% CO_2 conditions overnight before LFS PM_{10} exposure (day −1).

Neat LFS PM_{10} was serially diluted (%vol/vol) in serum-starved myocyte growth medium (0.5% fetal calf serum) (#C-22170; PromoCell) to the following concentrations: 10%, 5%, 3%, 2.5%, 2%, 1.5%, 1.25%, 1%, 0.75%, 0.5%, and 0% (PBS; vehicle). Serially diluted LFS PM_{10} was then added to wells (triplicates per concentrations) and incubated in an incubator at 37°C under 5% CO_2 conditions for up to 72 hours. For each day, the culture media were replaced with fresh serially diluted LFS PM_{10}. After 72 hours (3 days), HCM were assessed for viability using the CellTiter-Glo Luminescent Cell Viability Assay (#G7571; Promega Corp, Madison, Wis) according to manufacturer's recommendations. Luminescence was measured using the BioTek Cytation 3 Cell Imaging Multimode Reader (Agilent Technologies, Inc).

REFERENCES

E1. Carbery M, MacFarlane GR, O'Connor W, Afrose S, Taylor H, Palanisami T. Baseline analysis of metal(loid)s on microplastics collected from the Australian shoreline using citizen science. Mar Pollut Bull 2020;152:110914.

E2. Bhagwat G, Carbery M, Anh Tran TK, Grainge I, O'Connor W, Palanisami T. Fingerprinting plastic-associated inorganic and organic matter on plastic aged in the marine environment for a decade. Environ Sci Technol 2021;55:7407-17.

E3. Data download facility: regional air quality. NSW Government Department of Planning and Environment. Available at: https://www.dpie.nsw.gov.au/air-quality/air-quality-data-services/data-download-facility. Accessed May 24, 2020.

E4. Zhang Z, Hu X, Zhang X, Zhu X, Zhu L, Chen L, et al. Lung protective ventilation in patients undergoing major surgery: a systematic review protocol. BMJ Open 2014;4:e004542.

E5. Profiles of Health, Australia, 2011-13: Height and Weight. Australian Bureau of Statistics. Available at: https://www.abs.gov.au/ausstats/abs@.nsf/lookup/4338.0mainfeatures212011-13. Accessed February 21, 2021.

E6. Ali MK, Kim RY, Brown AC, Donovan C, Vanka KS, Mayall JR, et al. Critical role for iron accumulation in the pathogenesis of fibrotic lung disease. J Pathol 2020;251:49-62.

E7. Donovan C, Seow HJ, Bourke JE, Vlahos R. Influenza A virus infection and cigarette smoke impair bronchodilator responsiveness to beta-adrenoceptor agonists in mouse lung. Clin Sci (Lond) 2016;130:829-37.

E8. Donovan C, Seow HJ, Royce SG, Bourke JE, Vlahos R. Alteration of airway reactivity and reduction of ryanodine receptor expression by cigarette smoke in mice. Am J Respir Cell Mol Biol 2015;53:471-8.

E9. Donovan C, Simoons M, Esposito J, Ni Cheong J, Fitzpatrick M, Bourke JE. Rosiglitazone is a superior bronchodilator compared to chloroquine and beta-adrenoceptor agonists in mouse lung slices. Respir Res 2014;15:29.

E10. Donovan C, Royce SG, Esposito J, Tran J, Ibrahim ZA, Tang ML, et al. Differential effects of allergen challenge on large and small airway reactivity in mice. PLoS One 2013;8:e74101.

E11. Bourke JE, Bai Y, Donovan C, Esposito JG, Tan X, Sanderson MJ. Novel small airway bronchodilator responses to rosiglitazone in mouse lung slices. Am J Respir Cell Mol Biol 2014;50:748-56.

E12. Delmotte P, Sanderson MJ. Ciliary beat frequency is maintained at a maximal rate in the small airways of mouse lung slices. Am J Respir Cell Mol Biol 2006;35:110-7.

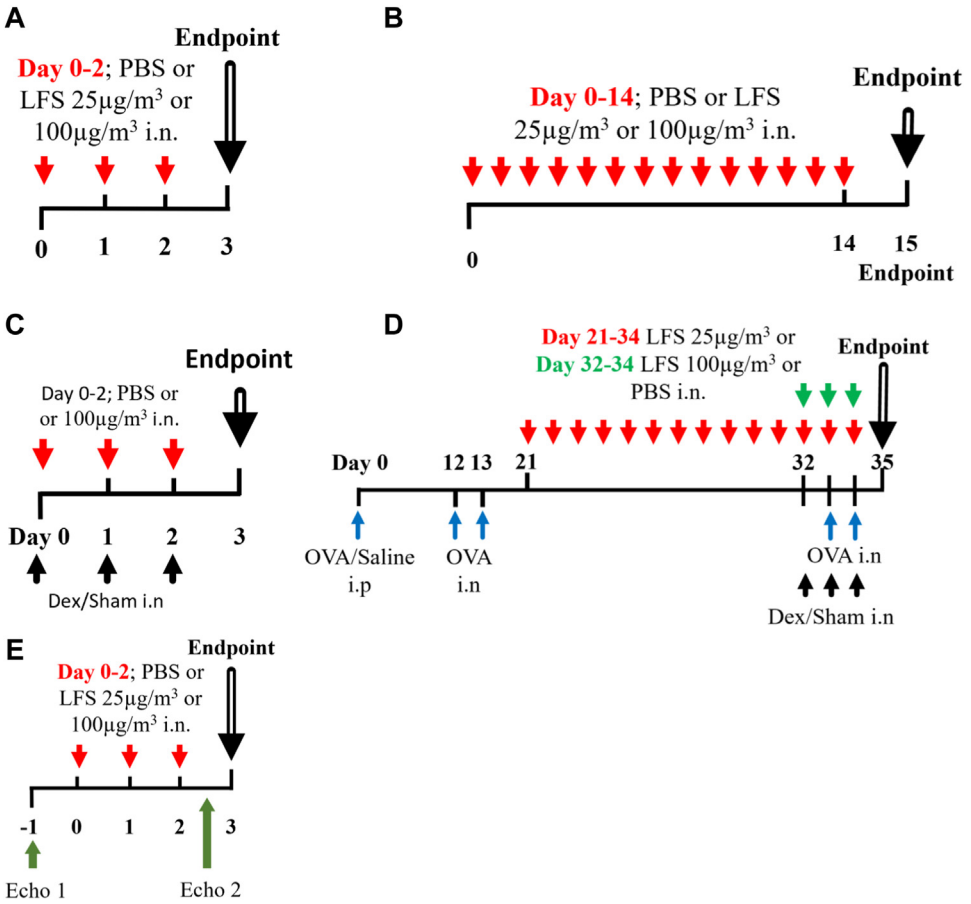

FIG E1. Experimental protocols for investigation of LFS PM_{10} airway exposure. **(A)** Model of short-term/low and moderate LFS PM_{10} airway exposure. Mice were intranasally administered PBS (control), 25 $\mu g/m^3$ LFS PM_{10} (daily equivalent), or 100 $\mu g/m^3$ LFS PM_{10} (daily equivalent) daily for 3 days. **(B)** Model of long-term/low and moderate LFS PM_{10} airway exposure. Mice were administered intranasally with PBS (control), 25 $\mu g/m^3$ LFS PM_{10} (daily equivalent), or 100 $\mu g/m^3$ LFS PM_{10} (daily equivalent) for 14 days. **(C)** Model of short-term and moderate LFS PM_{10} airway exposure with DEX treatment. Mice were intranasally administered PBS (control) or 100 $\mu g/m^3$ LFS PM_{10} (daily equivalent) with or without DEX treatment daily for 3 days. **(D)** Model of short-term/moderate and long-term/low LFS PM_{10} airway exposure on OVA-induced allergic airway disease. Mice were intraperitoneally sensitized to OVA (day 0), and allergic airway disease was induced by intranasal OVA challenge (days 12, 13) followed by re-challenge (days 33, 34). Nonallergic controls were sham-sensitized with saline. Steroid responses were assessed by intranasal treatment with DEX (days 32-34). Some groups were administered with 100 $\mu g/m^3$ (daily equivalent) short-term/moderate LFS PM_{10} (days 32-34), 25 $\mu g/m^3$ (daily equivalent) long-term/low concentration LFS PM_{10} (days 21-34), or PBS (control). **(E)** Model of short-term/moderate LFS PM_{10} airway exposure *(A)*. Echocardiography measures were obtained before mice were administered intranasally with PBS (control) or 100 $\mu g/m^3$ LFS PM_{10} (daily equivalent) for 3 days. A second echocardiography measure was obtained before end point. *i.n.,* Intranasal; *i.p.,* intraperitoneal.

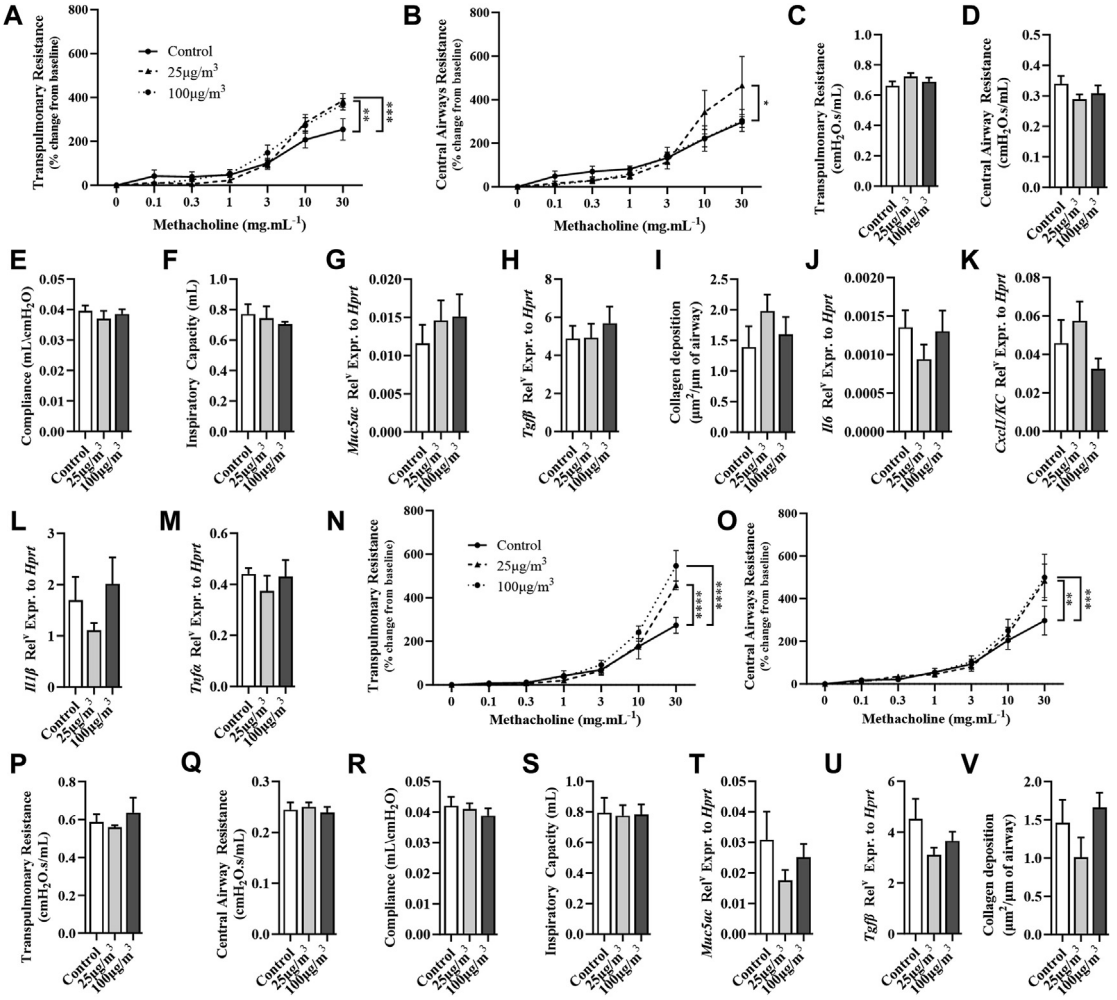

FIG E2. Lung structure, baseline lung function, and gene expression were measured in short- and long-term models of LFS exposure. In a model of short-term LFS PM_{10} airway exposure, AHR was measured in terms of **(A)** central airway resistance (percentage change from baseline) and **(B)** transpulmonary resistance (percentage change from baseline). Baseline lung function was measured in terms of **(C)** transpulmonary resistance, **(D)** central airway resistance, **(E)** compliance, and **(F)** inspiratory capacity. mRNA expression of **(G)** *Muc5ac* and **(H)** *Tgfβ* was measured in whole lung homogenate. Changes in lung structure were measured in terms of **(I)** collagen deposition around the small airway. Cells were isolated from BAL of short-term, moderate LFS PM_{10} airway exposure mice, and mRNA expression of **(J)** *Il6*, **(K)** *Cxcl1/KC*, **(L)** *Il1β*, and **(M)** *Tnfα* was assessed. In a model of long-term LFS PM_{10} airway exposure, AHR was measured in terms of **(N)** central airway resistance (percentage change from baseline) and **(O)** transpulmonary resistance (percentage change from baseline). Baseline lung function was measured in terms of **(P)** transpulmonary resistance, **(Q)** central airway resistance, **(R)** compliance, and **(S)** inspiratory capacity. mRNA expression of **(T)** *Muc5ac* and **(U)** *Tgfβ* was measured in whole lung homogenate. Changes in lung structure were measured in terms of **(V)** collagen deposition around the small airway. Unpaired *t* test was performed on LFS PM_{10} groups compared with controls. AHR data were assessed using 2-way ANOVA with Tukey *post hoc* test. n = 5-6/group. Data presented as mean ± SEM. **P* < .05, ***P* < .01, ****P* < .001, *****P* < .0001.

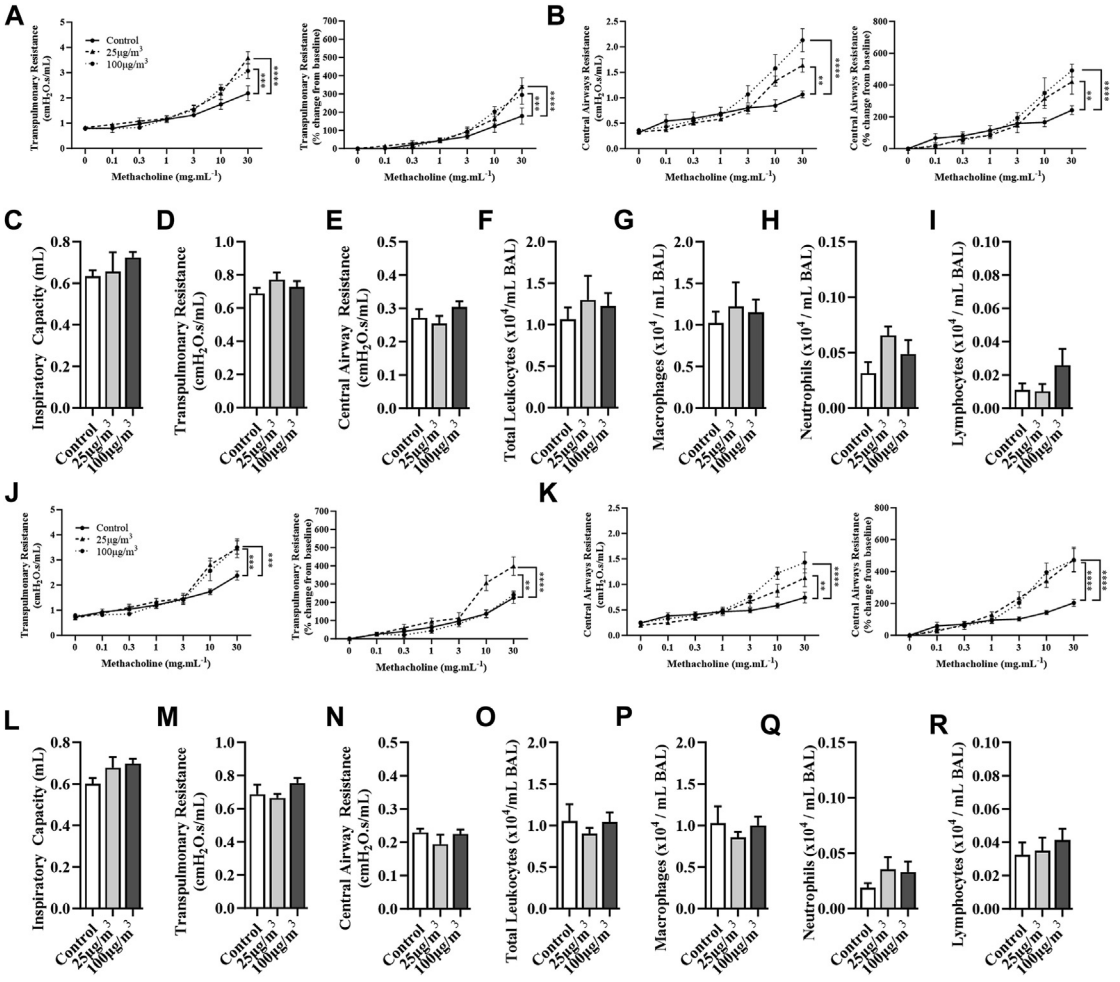

FIG E3. AHR, baseline lung function, and inflammation were measured in short- and long-term models of LFS exposure from a second sample (fuel source 2) LFS PM_{10}. In a model of short-term LFS PM_{10} airways exposure, AHR was measured in terms of **(A)** transpulmonary resistance and transpulmonary resistance (percentage change from baseline) and **(B)** central airway resistance and central airway resistance (percentage change from baseline). Baseline lung function was measured in terms of **(C)** inspiratory capacity, **(D)** transpulmonary resistance, and **(E)** central airway resistance. Inflammatory cells were measured in BAL in terms of **(F)** total leukocytes, **(G)** macrophages, **(H)** neutrophils, and **(I)** lymphocytes. In a model of long-term LFS PM_{10} airways exposure, AHR was measured in terms of **(J)** transpulmonary resistance and transpulmonary resistance (percentage change from baseline) and **(K)** central airway resistance and central airway resistance (percentage change from baseline). Baseline lung function was measured in terms of **(L)** inspiratory capacity, **(M)** transpulmonary resistance, and **(N)** central airway resistance. Inflammatory cells were measured in BAL in terms of **(O)** total leukocytes, **(P)** macrophages, **(Q)** neutrophils, and **(R)** lymphocytes. Unpaired *t* test was performed on LFS PM_{10} groups compared with controls. AHR data were assessed using 2-way ANOVA with Tukey *post hoc* test. n = 5-6/group. Data presented as mean ± SEM. $^{**}P < .01$, $^{***}P < .001$, $^{****}P < .0001$.

TABLE E1. SYBR Green primer sequences for gene expression studies

Gene	Forward (5′ → 3′)	Reverse (5′ → 3′)
Hprt	GCAGTTGTGTCACCATCATCTGTG	GGGGCAGTCTTGACTAACCCTCTT
Ppia	GGCAAATGCTGGACCAAAC	CATTCCTGGACCCAAAACG
Ahr	CACATCCGCATGATTAAGAC	TACTTCGCTTCTGTAAATGC
Cat	CTCCATCAGGTTTCTTTCTTG	CAACAGGCAAGTTTTTGATG
Il1β	TGGGATCCTCTCCAGCCAAGC	AGCCCTTCATCTTTTGGGGTCCG
Il4	CTGGATTCATCGATAAGCTG	TTTGCATGATGCTCTTTAGG
Il6	AGAAAACAATCTGAAACTTCCAGAGAT	GAAGACCAGAGGAAATTTTCAATAGG
Cxcl1/KC	AAGGAAGTGATAGCAGTCCCAAA	GCCAACAGTAGCCTTCACCC
Il13	AGACTCCCCTGTGCAACGGCA	GGAGACCGTAGTGGGGGCCTT
Muc5ac	GCAGTTGTGTCACCATCATCTGTG	GGGGCAGTCTTGACTAACCCTCTT
Myh7	GATGATCTATACCTACTCGGG	TGATGAGGATGGACTGATTC
Nppa	GAGAGAAAGAAACCAGAGTG	GTCTAGCAGGTTCTTGAAATC
Sod1	CACTCTAAGAAACATGGTGG	GATCACACGATCTTCAATGG
Sod2	CCATTTTCTGGACAAACCTG	GACCTTGCTCCTTATTGAAG
Tgfβ	CCCGAAGCGGACTACTATGCTA	GGTAACGCCAGGAATTGTTGCTAT
Tnfα	TCTGTCTACTGAACTTCGGGGTGA	TTGTCTTTGAGATCCATGCCGTT